Article

Electronic Structure, Magnetic Ordering, and Formation Pathway of the Transition Metal Oxide Hydride LaSrCoOH

Craig A. Bridges, George R. Darling, Michael A. Hayward, and Matthew J. Rosseinsky

J. Am. Chem. Soc., **2005**, 127 (16), 5996-6011• DOI: 10.1021/ja042683e • Publication Date (Web): 02 April 2005

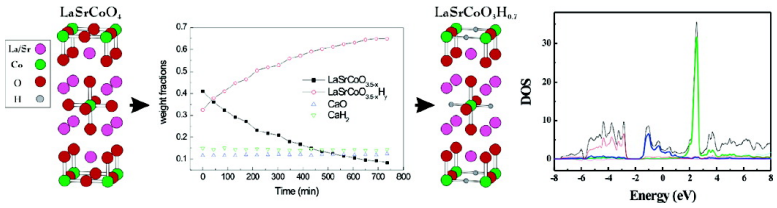

More About This Article

Additional resources and features associated with this article are available within the HTML version:

- Supporting Information
- Access to high resolution figures
- Links to articles and content related to this article
- Copyright permission to reproduce figures and/or text from this article

View the Full Text HTML

J|A|C|S
ARTICLES
Published on Web 04/02/2005

Electronic Structure, Magnetic Ordering, and Formation Pathway of the Transition Metal Oxide Hydride $LaSrCoO_3H_{0.7}$

Craig A. Bridges, George R. Darling, Michael A. Hayward,† and Matthew J. Rosseinsky*

Contribution from the Department of Chemistry, The University of Liverpool, Liverpool L69 7ZD, UK

Received December 6, 2004; E-mail: m.j.rosseinsky@liv.ac.uk

Abstract: The role of the hydride anion in controlling the electronic properties of the transition metal oxide hydride $LaSrCoO_3H_{0.7}$ is investigated theoretically by full potential DFT band structure calculation and experimentally by determination of the Néel temperature for three-dimensional magnetic ordering. The mechanism by which hydrogen is introduced into the solid is addressed by in situ X-ray diffraction studies of the formation of the oxide hydride, which reveal both a relationship between the microscopic growth of the observed oxide hydride order and the anisotropic broadening of the diffraction profile, and the existence of a range of intermediate compositions.

Introduction

The covalent interaction between transition metal cations and main group anions controls the localization, crystal field splitting, and resultant cooperative properties of the d electrons at the metal center. Extended arrays of first transition series cations bridged by the oxide anion support academically challenging and technologically important properties such as high-temperature superconductivity, colossal magnetoresistance, and ferroelectricity. The development of synthetic strategies giving access to such interacting arrays of metal centers bridged by other anions is thus an important task. The use of multiple anions in the oxide halide[1−3] and oxide chalcogenide[4,5] families produces electronic properties and chemical reactivities that are subtly altered from the oxides. The H^- hydride anion would be an interesting component of a multianion oxide-based system as it has bonding characteristics that can vary between ionic and covalent. However, the strong reducing power of the hydride anion ($E°(H^-/H_2)$ is estimated as −2.2 V) produces synthetic difficulties for classical high-temperature syntheses of target transition metal oxide hydrides due to competition from direct reduction to the metal, suggesting that lower-temperature kinetically controlled routes to such materials will be required. Current interest in the electronic state of hydrogen in semiconductors[6] and hydrogen-transporting transition metal oxides[7] has focused attention on the difficulty of studying negatively charged H-derived species in extended transition metal solids due to the low concentrations in which they occur, and it is therefore important to isolate oxide-based materials in which hydride occurs in sufficient concentration to allow both theoretical and experimental methods to probe its chemical nature.

Cobalt adopts a wide range of oxidation states, coordination environments, and electronic configurations in oxide systems.[8] The Co(III) phase $LaSrCoO_4$ adopts the tetragonal layered $n = 1$ Ruddlesden−Popper structure in which CoO_2 layers constructed from corner-sharing CoO_4 square units are separated by pairs of $(La_{0.5}Sr_{0.5})O$ layers, resulting in CoO_6 octahedra linked in two dimensions by corner-sharing. This phase is reduced by hydrogen to $LaSrCoO_{3.50,}$ with oxygen removed from the CoO_2 layer of the parent compound.[9] The more powerful hydride anion reducing agent NaH at 200 °C removes more oxygen to form $LaSrCoO_{3.38(2)}$, producing a significant concentration of Co(I). Both these reduced oxides remain tetragonal due to vacancy disorder in the perovskite layer. Increasing the reaction temperature to 450 °C, with CaH_2 as the reducing agent, resulted in the novel oxide hydride $LaSrCoO_3H_{0.70(2)}$ (**1**).[10] This reaction involves reduction of the Co and ordered substitution of oxide in the CoO_2 layers by hydride, forming chains of CoO_4 squares linked into a two-dimensional $CoOH_x$ array by hydride anions (Figure 1). **1** adopts an orthorhombic structure due to the ordering of oxide and hydride anions along orthogonal directions in the $CoOH_{0.7}$ plane. It is notable that this route avoids direct reduction to the metal and preserves the layered

† Current address: Inorganic Chemistry Laboratory, University of Oxford, South Parks Road, Oxford, OX1 3QR.

(1) Loureiro, S. M.; Felser, C.; Huang, Q.; Cava, R. J. *Chem. Mat.* **2000**, *12*, 3181−3185.
(2) Knee, C. S.; Price, D. J.; Lees, M. R.; Weller, M. T. *Phys. Rev. B* **2003**, *68*, 174407−174414.
(3) James, A. C. W. P.; Zahurak, S. M.; Murphy, D. W. *Nature* **1989**, *338*, 240−241.
(4) Hyett, G.; Rutt, O. J.; Gál, Z. A.; Denis, S. G.; Hayward, M. A.; Clarke, S. J. *J. Am. Chem. Soc.* **2004**, *126*, 1980−1991.
(5) Ijjaali, I.; Haynes, C. L.; McFarland, A. D.; Duyne, R. P. V.; Ibers, J. A. *J. Solid State Chem.* **2003**, *172*, 257−260.
(6) Cox, S. F. J. *J. Phys. Condens. Matter* **2003**, *15* (46), R1727−R1780.
(7) Wideroe, M.; Munch, W.; Larring, Y.; Norby, T. *Solid State Ionics* **2002**, *154*, 669−677.
(8) Hu, Z.; Wu, H.; Haverkort, M. W.; Hsieh, H. H.; Lin, H. J.; Lorenz, T.; Baier, J.; Reichl, A.; Bonn, I.; Felser, C.; Tanaka, A.; Chen, C. T.; Tjeng, L. H. *Phys. Rev. Lett.* **2004**, *92* (20), art. no.-207402.
(9) Hayward, M. A.; Rosseinsky, M. J. *Chem. Mater.* **2000**, *12*, 2182−2195.
(10) Hayward, M. A.; Cussen, E. J.; Claridge, J. B.; Bieringer, M.; Rosseinsky, M. J.; Kiely, C. J.; Blundell, S. J.; Marshall, I. M.; Pratt, F. L. *Science* **2002**, *295*, 1882−1884.

10.1021/ja042683e CCC: $30.25

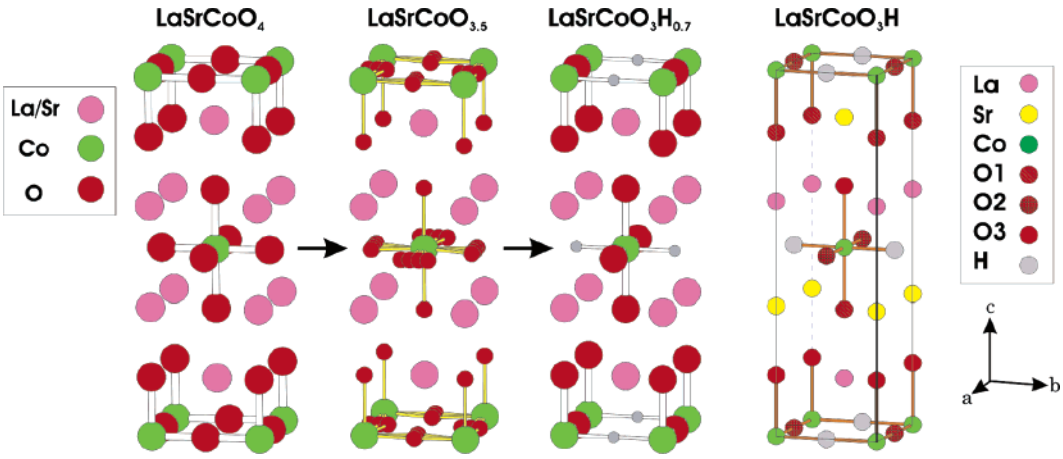

Figure 1. Formation of $LaSrCoO_3H$ via reduction of $LaSrCoO_4$. The unit cell on the far right is the *Imm*2 cell of $LaSrCoO_3H$ used with FPLAPW calculations to produce the DOS and bandstructure plots. Each oxygen anion is coordinated to a mixture of lanthanum and strontium cations.

structural features of the starting material. Although solid oxide hydrides containing main group,[11] lanthanide,[12] and actinide[13] elements are known, the observation of an extended transition metal oxide hydride is unprecedented.

The low-temperature transformation of oxide to oxide hydride contrasts with the more forcing high-temperature direct combination or substitution routes used to access other mixed anion solids[2] and raises significant questions concerning the reaction pathway leading to **1**. Here we report detailed in situ synchrotron powder X-ray diffraction measurements from room temperature to the reaction temperature, which reveal a surprisingly complex formation mechanism, in which the structures of the materials involved in the transformation evolve during the complete formation of **1**. Given the differences in size and valence electron configuration between O^{2-} $2s^22p^6$ oxide and $1s^2$ H^- hydride, both the nature and origin of the electronic properties of **1** compared to those of oxides are of fundamental interest. The coexistence of H^- and Co^{2+} centers is an interesting aspect of the electronic structure and resulting stability of **1** and suggests comparison with both salt-like[14,15] and intermetallic[16,17] hydrides. In this contribution, the strength and nature of the electronic interactions in the oxide hydride are revealed by determination of the magnetic ordering temperature. These studies are complimented by full potential band structure calculations on **1** and comparison with $LaSrCoO_4$, which are essential to understand the bonding and electronic properties of the materials by permitting quantitative evaluation of the role of the hydrogen orbitals in the electronic structure of **1** in comparison with an oxide of related structure.

Experimental Section

Synthesis. The citrate precursor method was used to prepare 5 g of $LaSrCoO_4$. La_2O_3 (99.999%, Aldrich), $SrCO_3$ (99.99%, Alfa Aesar), and cobalt powder (99.998%, Alfa Aesar) were weighed out in stoichiometric quantities and dissolved in dilute nitric acid with approximately 10 g of citric acid. This solution was then dried on a hot plate, and the resulting resin was decomposed at 700 °C overnight. To complete the preparation, the partially reacted powder was pelletized and fired for 48 h in air at 1200 °C, with one intermediate regrinding. The resulting product was pure by laboratory X-ray diffraction.

Caution! Reactions with CaH_2 generate hydrogen pressure within sealed Pyrex tubes. Unless otherwise stated, we work with Pyrex tubes that have a 12-mm outer diameter and a wall thickness of 1.5 mm and that are sealed under high vacuum (10^{-4} mbar). Maximum pressures of hydrogen gas in the tube at the reaction temperature are calculated to fall in the range of 1−55 bar for various samples detailed below (tubes of length ranging from 15 to 20 cm).

To obtain $LaSrCoO_3H_{0.70(2)}$ (sample A) for variable-temperature neutron diffraction studies, $LaSrCoO_4$ was mixed with CaH_2 (90−95%, Aldrich) [1:2 mole ratio] in a helium-filled glovebox. The mixture was sealed in a Pyrex tube under dynamic vacuum, followed by reaction at 450 °C for 48 h. After the reaction had gone to completion, the CaO reaction product and excess CaH_2 were washed out of the reaction product using a 0.1 M NH_4Cl solution in previously dried methanol on a Schlenk line.

Sample B was prepared for synchrotron X-ray diffraction in a 0.5-mm Pyrex capillary containing $LaSrCoO_4$ and CaH_2 [1:2.2 mole ratio] that was fired at 340 °C for 15 h and then quenched by removing the capillary from the furnace. Data were collected at room temperature on Station 9.1 of the SRS, Daresbury Laboratories, at a wavelength of 0.80550(1)Å.

A 1-g sample of $LaSrCoO_{3.5-x}$ was prepared by placing $LaSrCoO_4$ into a tube furnace, contained within an alumina boat, followed by reaction with 8% H_2 in nitrogen at 550 °C for 5 h. This was mixed with CaH_2 in a 1:2.2 mole ratio, sealed in a Pyrex tube under vacuum and heated at 450 °C for 12 h to produce sample C.

The product from a 2 g reaction between $LaSrCoO_4$ and CaH_2 [1:2]—formed at 450 °C for 48 h in a sealed tube—was washed using a 0.1 M solution of NH_4Cl in previously dried methanol on a Schlenk line. This was followed by annealing at 450 °C in an evacuated silica tube for 3 days (sample D).

From a single mixture of $LaSrCoO_4$ and CaH_2 [1:2.2 mole ratio], 0.05 g (2×) and 0.8 g (2×) of mixture were placed into four identical Pyrex tubes, which were then sealed off to the same volume under dynamic vacuum. Each Pyrex tube had been previously flame-heated under dynamic vacuum to remove adsorbed moisture. Two tubes, one containing 0.05 g (E) and the other 0.8 g (F) of the reaction mixture, were placed in the same furnace and ramped at 0.5 °C/min to 270 °C (held at this temperature for 5 h) and then at 0.3 °C/min to 450 °C (held at this temperature for 12 h). The other 0.05 g (G) and 0.8 g (sample H) samples were heated together in the same furnace at 5 °C/min to 450 °C, where the temperature was held for 12 h.

(11) Huang, B. Q.; Corbett, J. D. *Inorg. Chem.* **1998**, *37*, 1892−1899.
(12) Malaman, B.; Brice, J. F. *J. Solid State Chem.* **1998**, *53*, 44−54.
(13) Haschke, J. M.; Allen, T. H. *J. Alloys Compd.* **2001**, *320*, 58−71.
(14) Bertheville, B.; Herrmannsdorfer, T.; Yvon, K. *J. Alloys Compd.* **2001**, *325*, L13−L16.
(15) Yvon, K.; Kohlmann, H.; Bertheville, B. *Chimia* **2001**, *55*, 505−509.
(16) Joubert, J.-M.; Latroche, M.; Cerny, R.; Percheron-Guegan, A.; Yvon, K. *J. Alloys Compd.* **2002**, *330*−*332*, 208−214.
(17) Hector, L. G.; Herbst, J. F. *Appl. Phys. Lett.* **2003**, *82*, 1042−1044.

A Pyrex tube containing an intimately mixed 0.5 g sample (I) of $LaSrCoO_4$ and CaH_2 [1:2.2 mole ratio] was fired at 450 °C for 15 h under dynamic vacuum ($\sim 1 \times 10^{-4}$ mbar).

A Pyrex tube containing an intimately mixed 1 g sample (J) of $LaSrCoO_4$ and CaH_2 [1:1.05 mole ratio] was sealed under vacuum, and then fired at 450 °C for 48 h.

Samples C−J were examined qualitatively using laboratory powder X-ray diffraction employing Co Kα radiation. Data of a quality suitable for Rietveld refinement were collected on sample D using a PANalytical X'pert Pro Multi-Purpose X-ray diffractometer employing Co $K\alpha_1$ radiation.

Thermogravimetric Measurements. A Seiko SII-TG/DTA 6300 thermal analyzer was used with a Hiden HPR 20 RGA mass spectrometer (He, H_2O, O_2, and CO_2 were monitored). Approximately 30 mg of washed (with 0.1 M NH_4Cl solution in methanol) sample J was loaded into an alumina crucible and heated at 5 °C min^{-1} under a flow of ∼20% O_2 in He (Air Products) from 20 to 840 °C. The quantitative response of the mass spectrometer to H_2O was calibrated using the decomposition of $CaC_2O_4 \cdot H_2O$.

Band Structure Calculations. The WIEN2K density functional theory code was used to carry out full-potential linearized-augmented plane wave (FPLAPW) band structure calculations, using the scalar-relativistic version without spin−orbit coupling.[18] Local orbitals have been included for La 5s, 5p, Sr 4s, 4p, Co 3p, and O 2s, and the PBE[19] version of gradient corrections to the LDA was applied. Tests indicated that 164k points in the irreducible part of the Brillouin zone (IBZ) were sufficient for convergence of the total energy. The total energy was converged to lower than 10^{-4} Ry/cell, and the charge to less than 10^{-4} electrons/atom. Experimental lattice constants and atomic positions were used for all calculations. The sphere radii used were La/Sr 2.25, Co 1.8, O 1.8, and H 1.4 bohr. The values for convergence of total energy and charge, as well as the sphere radii, apply to calculations on $LaSrCoO_4$ and $LaSrCoO_3H$.

The structural models used for the calculations of both $LaSrCoO_3H$ and $LaSrCoO_4$ require consideration of the disordered occupation of the A sites by La and Sr cations in these materials. For $LaSrCoO_3H$ the symmetry was lowered from *Immm* to *Imm*2, splitting the 4*i* position of *Immm* into separate 2*a* La^{3+} and Sr^{2+} positions in *Imm*2 (Figure 1). The 4*i* position of O1 is also split into two oxygen sites (O1 and O3). The local environment of the O1 and O3 sites now differ, as is not the case in the experimentally determined structure, in which La^{3+} and Sr^{2+} are randomly distributed with a range of local environments.

To examine the effect of altering the symmetry on the DOS, the symmetry was further lowered to *Pmm*2, and Wien2K calculations were run using the same parameters as for $LaSrCoO_3H$. Two sites are present in the *Pmm*2 space group setting for each of the sites in *Imm*2 symmetry, and two La^{3+}/Sr^{2+} distributions distinct from *Imm*2 are possible (Figure S1). In the first, each perovskite layer contains only one type of A cation, with an alternation of La^{3+} and Sr^{2+} containing perovskite layers along the *c* axis; calculations on this structure type were extremely difficult to converge with the set of parameters used in the *Imm*2 calculations. In the second, each rocksalt layer contains only one type of A cation, with an alternation of La^{3+} and Sr^{2+} containing rocksalt layers along the *c* axis; calculations on this structure type were converged with the set of parameters used in the *Imm*2 calculations.

The structural model used for $LaSrCoO_4$ is identical to the *Imm*2 model used for $LaSrCoO_3H$, with the exception that the H^- anion has been substituted with an oxygen anion (labeled O4) in the plane of the perovskite layer (Figure 1). This required lowering the symmetry from tetragonal *I*4/*mmm* to orthorhombic *Imm*2, while maintaining the tetragonal cell constants at experimental values.[20]

Neutron Diffraction. Measurements were performed on a 1-g sample sealed under helium in a vanadium can, employing a copper O-ring to provide a seal at all temperatures. Data were collected over a range from 0° to 140° (2θ) on the D20 diffractometer at the Institute Laue-Langevin, Grenoble. The temperature program involved a continuous ramp from 2 to 320 K (ramp of 0.004 K/s, scan time of 9 min) in an orange cryostat, then from 296 to 432 K (with the same ramp and scan times) using the ILL vacuum furnace. These patterns were later summed to produce data from 6 to 320 K in 6 K steps, and from 299 to 429 K in 6 K steps.[21]

The D2B diffractometer was used to collect high-resolution data at 345, 360, 375, 390, and 405 K in a cryofurnace, employing a wavelength of 1.59478(1) Å as calibrated using CeO_2 NIST standard.

The D20 data were initially refined using an estimated wavelength of 1.301Å. The D20 data were then scaled to fit with data collected using the same sample on D2B, as the wavelength calibration for the D2B data is much more precise. The cell parameters for data collected at 345 K on D2B were held constant during a wavelength refinement of 346 K data from D20, obtained during the ramp from 296 K in the ILL vacuum furnace. The wavelength obtained by this procedure, 1.29774(4) Å, was used to refine D20 data at 6, 49, 89, 130, 171, 213, 254, 296, and 320 K. The D20 data at all temperatures collected with the orange cryostat were then scaled to agree with the data refined at 1.29774(4)Å. Temperature readings from the furnace were obtained by placing a thermocouple in contact with the sample can, while ensuring that the thermocouple remained outside of the neutron beam.

In Situ Synchrotron X-ray Diffraction. Experiments were performed on Station 9.1, a high angular resolution powder diffraction facility, of the Synchrotron Radiation Source (SRS), Daresbury Laboratory, UK. On this station, a 5 T wiggler is used to produce X-ray radiation in the energy range 7−30 keV. A Si 111 monochromator was used to select a radiation of 0.8000(1) Å wavelength, chosen to avoid fluorescence problems below the absorption edge of Sr (16.1keV; 0.77 Å). The wavelength and zero-point offset were determined accurately, using the Bragg reflections of an NBS silicon standard. An intimately ground mixture of $LaSrCoO_4$ and CaH_2 [1:2.2 mole ratio] was sealed under helium gas (1 bar of pressure) in 0.5-mm Pyrex capillaries. Results from capillaries that were filled less than 50% are presented below, as completely filled capillaries were found to explode at the reaction temperature from the pressure of evolved H_2 gas during ramping to 450 °C. Data were obtained using a conventional two-circle diffractometer in Debye−Scherrer geometry. A furnace was used which provided a maximum accessible temperature above 600 °C and a temperature stability of ±10 °C at 450 °C. The temperature stability and average temperature were determined by collecting a series of measurements using a thermocouple placed at the capillary position, while holding at a given setpoint on the temperature controller. For the first in situ experiment (capillary 1) the temperature was ramped in stages, with a 5° C/min ramp rate between temperatures: 19 °C for 2 h, 140 °C for 3 h, 240 °C for 35 min, 290 °C for 20 min, 340 °C for 3.5 h, 400 °C for 5 h, 415 °C for 40 min, 450 °C for 13 h, 475 °C for 3 h, and 500 °C for 4 h.

At the temperatures at which the sample was held for over 1 h, extended data sets suitable for Rietveld refinement were collected. Data were collected for 4.3 min (15.5−18° 2θ; 0.01° 2θ step size; up to 340 °C) or 5.2 min (15−18° 2θ; 0.01° 2θ step size; above 340 °C) during the shorter periods of temperature stability. The region examined by the shorter scans contained the most intense peaks of $LaSrCoO_4$, $LaSrCoO_{3.5-x}$, $LaSrCoO_3H_y$, and CaH_2, which rapidly revealed the

(18) Blaha, P.; Schwarz, K.; Madsen, G. K. H.; Kvasnicka, D.; Luitz, J. *WIEN2k*, An Augmented Plane Wave Plus Local Orbitals Program for Calculating Crystal Properties; Vienna University of Technology: Austria, 2001.
(19) Perdew, J. P.; Burke, K.; Ernzerhof, M. *Phys. Rev. Lett.* **1996**, *77*, 3865−3868.
(20) Demazeau, G.; Courbin, P.; Flem, G. l.; Pouchard, M.; Hagenmuller, P.; Soubeyroux, J. L.; Main, I. G.; Robins, G. A. *Nouv. J. Chim.* **1979**, *3*, 171−174.
(21) During the initial stages of each ramp, the temperature increase deviated slightly from the programmed ramp rate. This has been taken into account in the average temperatures reported for the summed D20 data.

progress of the reaction to form the oxide hydride. The 400 and 450 °C diffractograms were each collected over a period of 43 min with an angular range of 35−10° 2θ, and a step size of 0.01° 2θ. The reaction occurred at a sufficiently slow rate that the data at these temperatures could be refined to extract cell constants and phase fractions. Data obtained at 475 and 500 °C were used to observe the completion of the reaction, as judged by the disappearance of the $LaSrCoO_{3.5-x}$ phase, as well as to examine the temperature stability of the oxide hydride **1**.

A further in situ experiment (capillary 2) was performed on an intimately ground mixture of $LaSrCoO_4$ and CaH_2 [1:1 mole ratio] that was sealed under helium gas (1 bar of pressure) in a 0.5-mm Pyrex capillary. This capillary was ramped from 125 to 550 °C at a rate of 0.5 °C/min. Data were collected at a scan time of 10.3 min over an angular range of 16−19° 2θ, with a step size of 0.01° 2θ.

In addition, five in situ experiments involving intimately ground mixtures of $LaSrCoO_4$ and CaH_2 at a 1:2.2 mole ratio have been examined to determine the reproducibility of the in situ results. Four different 0.5-mm Pyrex capillaries (capillaries 3−6) containing this mixture of reagents were sealed under helium gas (1 bar of pressure) and placed in the furnace at Station 9.1. The fifth capillary (capillary 7) was a 0.5-mm quartz capillary sealed under the same conditions and containing the same reaction mixture. Details of the temperature programs used for these capillaries are given in the Supporting Information.

Rietveld refinement was performed using the GSAS suite of programs for all of the X-ray and neutron diffraction patterns.[22]

Results

Figure 2a displays the total density of states (DOS) for $LaSrCoO_3H$. The first point to address is that the FPLAPW results in this study indicate that $LaSrCoO_3H$ is metallic, contrary to expectations from experiment, which shows an ordered antiferromagnetic insulator at room temperature. This is because the material is a Mott−Hubbard insulator in which the interelectron repulsion U localizes the 3d electrons—U is not included in the present calculations.

Our aim in performing these calculations is to compare the bonding interactions conferring stability on oxide hydrides with those in oxides rather than ab initio prediction of electronic properties, and it is thus the distribution of initial atomic states in the final electronic structure of **1** over the entire valence region rather than the existence of a gap at E_F that is our focus here.

The La 4f states are concentrated in a sharp peak approximately 2.5 eV above the Fermi level, with the 5d states of La, and the Sr 5s states spreading to higher energies. While the La and Sr states mainly contribute to unoccupied states in the conduction band, the cobalt cation states mix significantly with its coordinating anions. The majority of the Co 3d states are located around the Fermi level, with some mixing into the predominantly oxygen 2p states from −2.5 to −5.7 eV.

As shown in Figure 3a, the Co t_{2g} orbitals largely sit just below the Fermi level, are relatively nonbonding, and mix into bands from −1.8 to 0.3 eV. These orbitals show some mixing with O *2*p states, but mix negligibly with H 1s due to its σ symmetry with respect to the metal−ligand bond. Figure 3b,c shows that the 3d e_g orbitals of Co mix strongly into the valence band, which is composed mainly of O 2p states between −2.2 and −7.6 eV. In the region of the Fermi level the Co $3d_{z^2}$ DOS

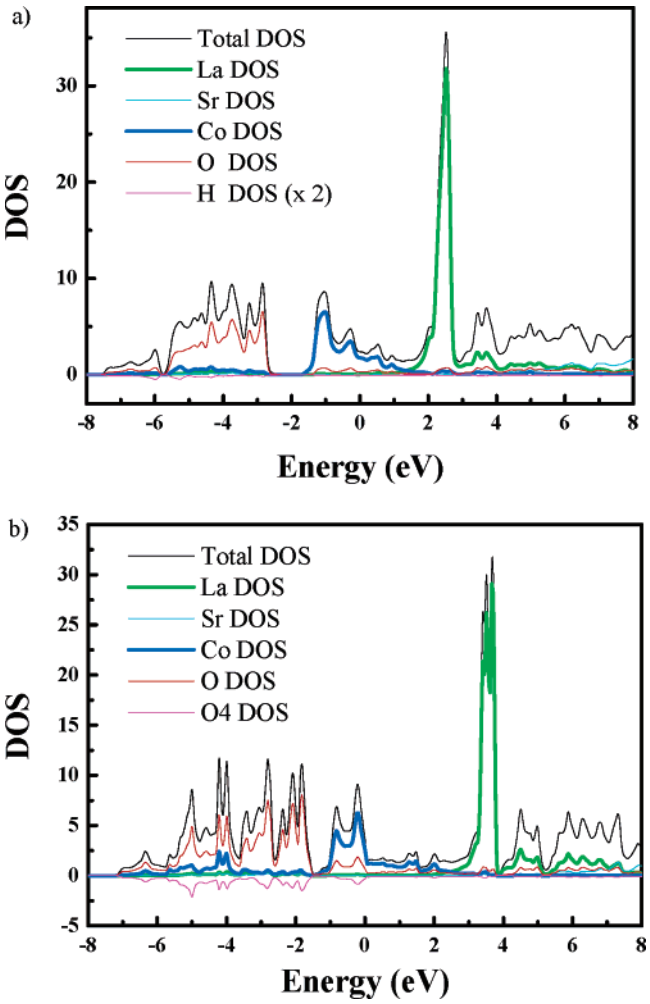

Figure 2. (a) The total density of states for $LaSrCoO_3H$. The projected density of states for La, Sr, Co, O, and H are shown. The H contribution has been multiplied by a factor of 2 to make it more visible. (b) The total density of states for $LaSrCoO_4$. The O4 anion occupies the same position as hydride H in the $LaSrCoO_3H$ structure.

contributions extend from −1.5 to 1.6 eV; the Co $3d_{x^2-y^2}$ DOS is broader, extending from −1.5 eV to above 3 eV. The $3d_{z^2}$ orbital is oriented toward both O1 and O3 along the *c* axis, and mixes mainly with the oxygen bands from −5.7 to −2.2 eV to produce a broad distribution of states. The $3d_{x^2-y^2}$ orbital mixes with the σ symmetry orbitals from the O2 and H anions. As a result, the region between −4.9 and −7.6 eV contains contributions from O2 2p, H 1s, and Co 3d e_g orbitals (Figure 3b−e). The comparison between z^2 and x^2-y^2 states reveals a more pronounced x^2-y^2 contribution (approximately double) at low energies (<−5.7 eV), suggesting greater mixing with the anion states at these energies and a stronger contribution to the in-plane bonding. There is also an admixture of Co 4s and 4p orbitals in the valence states, in particular into the low-energy region where H 1s is prevalent (Figure S2). The Co 4s and $3d_{x^2-y^2}$ contributions are approximately equal, while the Co 4p contribution is ∼1/3 that of $3d_{x^2-y^2}$ in the <−5.7 eV region.[23] Due to the mixing of the x^2-y^2 3d orbital into the low energy

(22) Larson, A. C.; von Dreele, R. B. *Los Alamos National Laboratory, Los Alamos, LANSCE* **1994**.

(23) These comparisons are based upon integration of the projected DOS in the specified energy range and therefore do not consider the DOS in the interstitial region. These figures may be considered rough estimates of the relative orbital contributions.

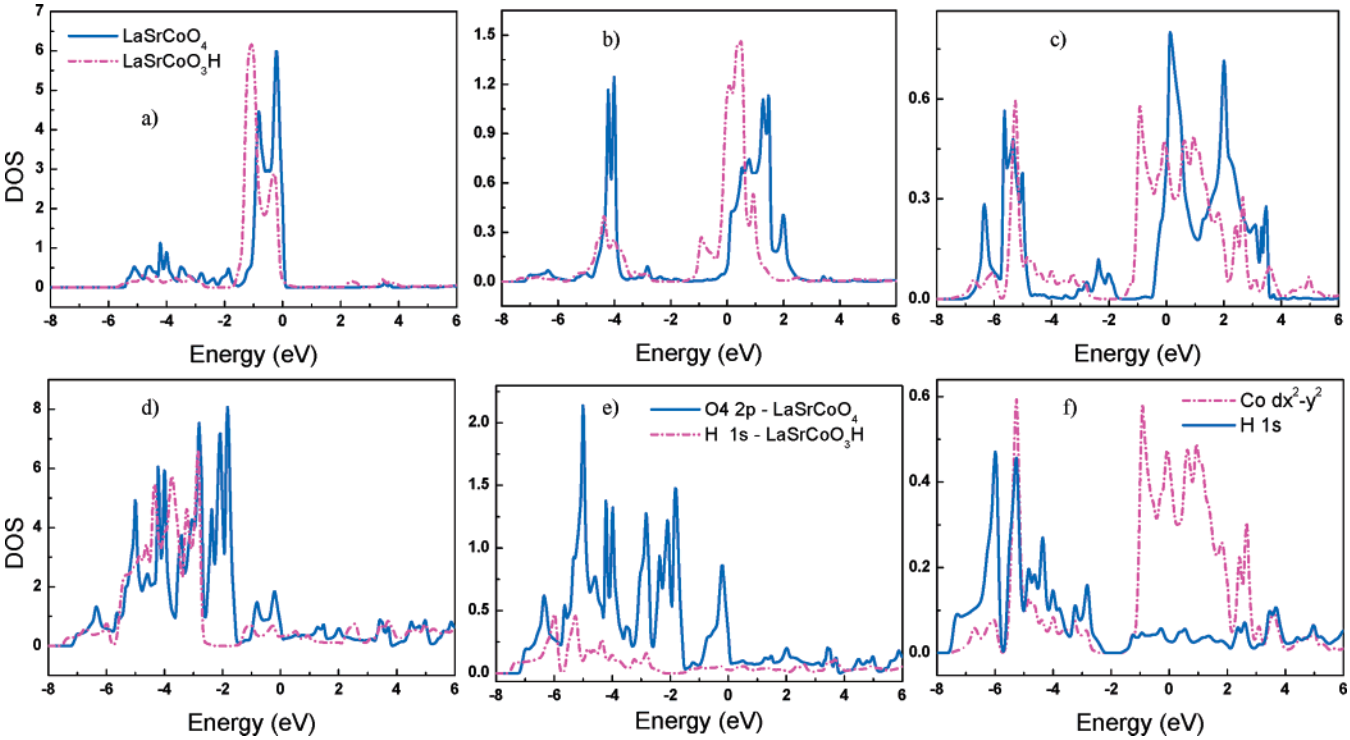

Figure 3. Comparison between the DOS of $LaSrCoO_4$ and $LaSrCoO_3H$: (a) Co t_{2g}, (b) Co $3d_{z^2}$, (c) Co $3d_{x^2-y^2}$, (d) O Total DOS, (e) O4 Total DOS and H 1s. Both DOS curves in plot (f), which displays Co $3d_{x^2-y^2}$ and H 1s states, pertain to $LaSrCoO_3H$.

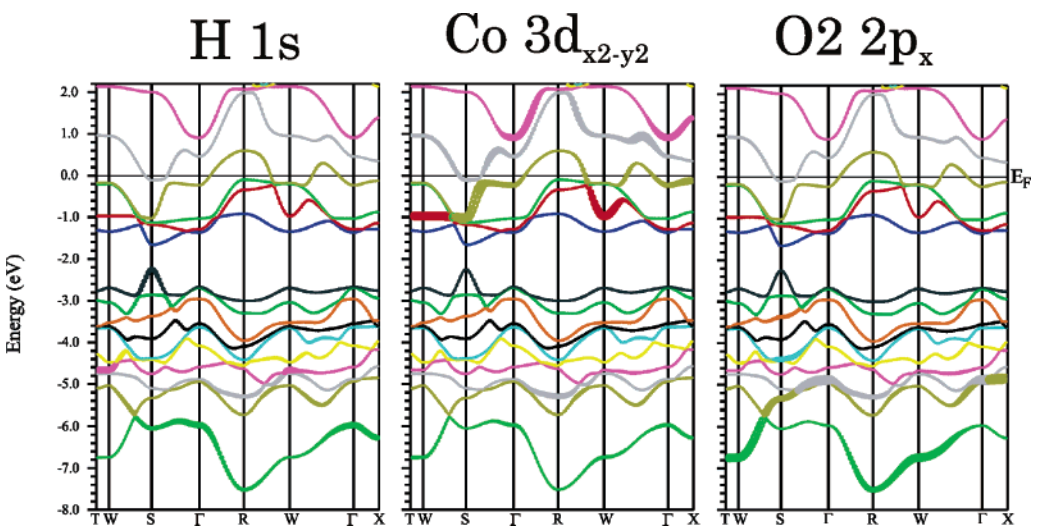

Figure 4. Bandstructure of $LaSrCoO_3H$ with band character plotting. The middle figure shows that though the majority of Co $3d_{x^2-y^2}$ character is in the region of the Fermi level, significant contributions are present at the bottom of the valence band along directions similar to those of the H 1s contributions, in particular, near Γ in the energy region of −6 eV. Most of the oxygen contribution in the lowest-energy band is from O2 $2p_x$ character, which is the orbital oriented in the direction of the cobalt cations.

anion states, the H 1s contribution is visible around E_F, where Co $3d_{x^2-y^2}$ and O 2p are present, as well as above E_F (Figure 3f).

To highlight the mixing of Co 3d, H 1s, and O2 2p states within the perovskite CoOH layer, the band structure has been plotted with atomic character of the band states in Figure 4. As apparent from the DOS in Figure 2a, the lowest-energy bands are predominantly anionic (H 1s and O 2p), with the main metal contributions coming from the Co $3d_{x^2-y^2}$ and 4s. The Co $3d_{x^2-y^2}$ and H 1s states clearly contribute to similar regions of the lowest-energy valence bands, in particular around Γ in the lowest band, where there is also a Co 4s contribution. These results may be expected from the symmetry arguments illustrated in Figure S3a, in which bonding between Co $3d_{x^2-y^2}$ and H 1s contrasts with O2 $2p_x$ nonbonding interactions. Similarly, mixing between Co 4s and H 1s may be expected around Γ on the basis of symmetry arguments. However, O2 $2p_x$ character is observed in the lowest band away from Γ, where symmetry does not restrict its mixing.

When the second *Pmm*2 La^{3+}/Sr^{2+} distribution (Figure S1) is compared with the *Imm*2 La^{3+}/Sr^{2+} distribution, significant energy shifts are observed in contributions to the valence band from the oxygen anions in the rocksalt layer (Figure S4a). The DOS for oxygen sites in the Sr^{2+} containing layer is shifted

higher in energy, toward the Fermi level, which nearly closes the gap between anion- and Co-derived bands that is present in the *Imm*2 calculation (Figure S4e). The DOS for oxygen sites in the La^{3+}-containing layer are shifted lower in energy, and away from the Fermi level (Figure S4f). However, the DOS of the cobalt cation, the hydride anion, and the oxygen anion within the perovskite layer are very similar in both calculations (Figure S4b−d). This indicates that the main conclusions drawn in this paper from the DFT results, which relate to Co−O and Co−H mixing, are unaffected by the lowering of symmetry from *Immm* to *Imm*2 or *Pmm*2.

The total DOS for the parent Co^{III} oxide $LaSrCoO_4$ is shown in Figure 2b. The features are strikingly similar to $LaSrCoO_3H$. Perhaps the most distinct difference between the electronic structures of the two compounds is that the (mainly 3d) states near the Fermi energy in $LaSrCoO_4$ are shifted lower in energy relative to the sharp peak of La^{3+} states (width of 2.8−3.8 eV), and closer to the top of the predominantly O 2p states (−7.6 to −1.5 eV). As a result, there exists a finite DOS between the valence and conduction bands, removing the gap that is present in the oxide hydride **1**. The shift in the Fermi level is due to a change in oxidation state: $LaSrCoO_4$ contains Co^{3+}, and thus one fewer d electron than the Co^{2+} cation in $LaSrCoO_3H$. The Fermi level is situated in the conduction band, near the bottom of the e_g states rather than being well into the x^2-y^2 states as in the oxide hydride (Figure 3a−c). Therefore, the calculation incorrectly predicts a metal, as for **1**.

The similarity of the DOS of $LaSrCoO_3H$ and $LaSrCoO_4$ indicates that the hydride anion is influencing the electronic structure in a manner similar to the in-plane oxide anion O4 that it replaces. This is most evident at the bottom of the valence band, where energy bands below −4.6 eV in both the oxide and the oxide hydride are composed of Co $3d_{x^2-y^2}$, O2 2p, and either O4 2p or H 1s character (Figure 3e). In this region there are additional contributions from Co $3d_{z^2}$, Co 4s, and Co 4p (Figure S2). It is interesting to note that the Co $3d_{x^2-y^2}$ width appears greater in the oxide hydride than in $LaSrCoO_4$. In $LaSrCoO_4$ the width extends from −0.5 to 3.5 eV, while the oxide hydride exhibits significant $3d_{x^2-y^2}$character from −1.5 to 4.0 eV.

The band structure of $LaSrCoO_4$ is shown in Figure S5. The shift in the Fermi energy is clearly visible. The bands exhibit symmetry around Γ due to the tetragonal structure. At Γ, replacing O 2p with H 1s means replacing a set of orbitals that are out of phase (and thus orthogonal to the e_g orbitals at Γ which are in-phase) with a set (H 1s) that are in phase and thus capable of bonding with Co. The two situations are shown in Figure S3.

An analysis of dispersion in the $LaSrCoO_3H$ bandstructure (Figure 4) along the Γ−S direction is as follows. From Γ, there is an initial increase in energy, followed by a further decrease in energy toward S. We attribute the initial increase to the fact that the H 1s orbitals are out of phase with the e_g orbitals along k_y (along the *b* axis of the direct space cell in Figure S3). The minor contribution of mixing between H 1s and Co 4s would not be affected by moving out of phase in this direction. At S, the main contributions are from H 1s and O2 $2p_y$;[24] these orbitals were out of phase at Γ, but are in phase at S. Thus, the further decrease in energy to S can be attributed to the mixing between H 1s and O2 $2p_y$. Further contributions at S come from the Co $4p_y$ orbital (visible in Figure 4 at −6 eV) and the axial oxygen orbitals O1 $2p_y$ and O3 $2p_y$.

In addition, there is a contribution to the decrease in energy along Γ−S from moving out of phase along the k_z direction, as the point S is out of phase along both k_z and k_y. Along Γ−X[25] the orbitals become out of phase along the reciprocal vector k_z. In the oxide hydride there is a significant decrease in energy at X, in contrast to the case of $LaSrCoO_4$ in which a very slight increase in energy is observed. The change in the band structure along Γ−S and Γ−X when comparing $LaSrCoO_4$ with $LaSrCoO_3H$ illustrates the significant effect of the H 1s symmetry on the electronic structure of the oxide hydride.

The structural model used to refine the neutron diffraction data has been described previously.[10] The refined phases include $LaSrCoO_3H_{0.7}$, La_2O_3, the vanadium can, and the magnetic structure of $LaSrCoO_3H_{0.7}$. One region of the D20 data was excluded (62.7−63.9°) due to the presence of an instrumental contribution. Similarly, there were weak peaks present in the D2B data arising from the cryofurnace that were excluded from the following regions: 38.79−42.34°, 65.7−66.6°, 68.6−69.5°, and 78.80−80.72°.

The magnetic structure was refined as a separate magnetic phase of symmetry P1. The magnitude and orientation of the ordered moment was constrained to be equal on all cobalt sites, with the antiferromagnetic interactions according to the previously determined magnetic structure.[10] The magnitude of the moment with increasing temperature was refined by using the fractional occupancy of the cobalt ions as a scaling factor, after having initially refined the moment at low temperature. The scaling factors of the chemical and magnetic cells were in the ratio 1:0.5, to compensate for the doubled volume of the magnetic cell. This resulted in a refined moment of 2.76(4)μ_B at 6 K.[26]

Previous reports of $LaSrCoO_3H_{0.7}$ indicated that the magnetic ordering temperature lies above 350 K. Figure 5 shows that the magnetic ordering temperature is 380 K. Critical exponent analysis of the magnetization data is given in Figure S6.

The relatively featureless evolution of cell constants (Figure S7) suggests that no structural phase transition occurs in this temperature region. Each of the axes increases steadily with increasing temperature. Figure S8 illustrates the smooth variation of the isotropic atomic displacement parameter for the hydride anion with temperature, indicating that the anion remains localized at its bridging site in the structure over the temperature range studied. Figure S9 shows Rietveld refinements of data collected using the higher-resolution diffractometer D2B. Thermal expansion is largest along *b* i.e., the direction of the Co−H bond.

The temperature-dependent data for each of the axes, as well as the volume, have been fitted with the Einstein equation to derive the phonon frequency. The data are presented as an inset to Figure S7. The Co−H bond would appear to be weaker than

(24) Though the main contribution at S is from O2 $2p_y$, this contribution is less than 20% of the total O2 2p contribution to the band in the energy region −7.6 to −5.7 eV. The main contribution is provided by the O2 $2p_x$ orbital, which points directly towards the cobalt cation within the perovskite layer.

(25) T ($^1/_2$, $^1/_2$, 0), W ($^1/_2$, $^1/_2$, $^1/_2$), S (0, $^1/_2$, $^1/_2$), G (0, 0, 0), R ($^1/_2$, 0, $^1/_2$), X (0, 0, $^1/_2$).

(26) The components of the moment for the Co atom at (0,0,0) were refined at 6 K, and are $m_x = 1.56(8)$, $m_y = 1.4(1)$ and $m_z = 1.79(8)$ μ_B. This differs from [10] as the scaling factors used for the chemical and magnetic cell in that study were in a ratio of 1:1. The correct scaling factors should be set at a ratio of 1:0.5.

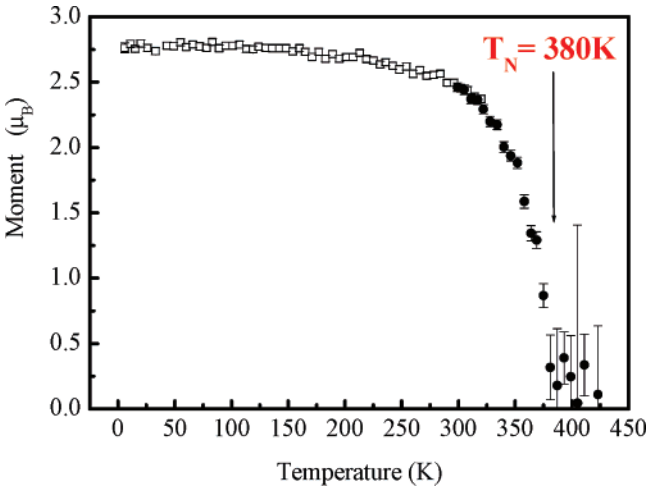

Figure 5. Temperature-dependent magnetic moment of $LaSrCoO_3H_{0.7}$. The magnetic ordering temperature is 380 K.

the Co−O bond from both the lower phonon frequency and the (related) thermal expansion along *b* (Table S10). The excellent fits to the Einstein equation over the full temperature range show that **1** is a well-behaved solid as a function of temperature and does not decompose, separate into closely related phases of similar composition, or undergo structural rearrangement over this temperature range.

The in situ X-ray diffraction study of the reaction between $LaSrCoO_4$ and CaH_2 provided information about reaction intermediates and kinetics, as well as the evolution of lattice parameters and phase fractions, which indicates whether the phases in question evolve in structure and/or composition during the formation of **1**. Although results from seven different capillaries are reported, capillary 1 has been studied in the greatest detail, and thus, the relevant stages of its temperature program are described here. The sample temperature was increased to initiate the reaction between $LaSrCoO_4$ and CaH_2, which produced CaO and the oxygen-deficient phase $LaSrCoO_{3.5-x}$ above 240 °C. The complete conversion of $LaSrCoO_4$ to $LaSrCoO_{3.5-x}$ was observed during a hold for 3.5 h at 340 °C, before the temperature was raised to 400 °C to initiate formation of $LaSrCoO_3H_y$. This was followed by a ramp to 450 °C to obtain the optimum reaction rate for data collection. Portions of the data collected during the conversion of $LaSrCoO_{3.5-x}$ into $LaSrCoO_3H_y$ at both 400 and 450 °C are displayed in Figure 6 and Figure S11. The temperature was then raised to complete the formation of oxide hydride. While weak peaks of $LaSrCoO_{3.5-x}$ remained after a 3 h period at 475 °C, a further treatment at 500 °C resulted in a mixture of $LaSrCoO_3H_y$, CaH_2, and CaO. No impurity peaks were observed during the 4 h hold at 500 °C, suggesting that the oxide-hydride phase **1** is stable at this temperature under the reaction conditions. An example of a Rietveld refinement of the data collected at 450 °C is given in Figure 6c. The figures of merit for this fit are typical of the fits to the in situ data.

Refinements at each temperature were based upon previously described crystal structures for $LaSrCoO_4$,[20] $LaSrCoO_{3.5-x}$,[9] $LaSrCoO_3H_{0.7}$,[10] CaH_2,[27] and CaO.[28] An approximate absorption coefficient was calculated on the basis of the initial composition and the capillary diameter, and was held constant throughout. As the absorption coefficient of the cobaltate material changes very little over the course of the reaction and provides the dominant contribution to the absorption of the mixture, the use of a fixed coefficient is expected to be an acceptable approximation. All data were normalized to monitor counts, and then scaled with the same scaling factor to ensure that the quantitative analysis would be valid. The absolute values of the phase fractions are sensitive to the absorption coefficient used, although the temperature evolution of the relative values should be reliable.

At 400 and 450 °C, the tetragonal reduced phase **2** (structurally analogous to $LaSrCoO_{3.5-x}$) is converted into **1**. The evolution of lattice parameters (capillary 1) has been quantified using Rietveld refinement for both disappearing **2** and forming **1**. These data are presented in Figures S12 (400 °C data) and 7 (450 °C data), along with the changes in weight fraction of each phase with time.

Over the 5 h hold at 400 °C no significant change was observed in the *a* or *b* lattice parameters of either phase. The peaks of the oxide-hydride phase are extremely broad, indicating that the crystallinity of the material is rather poor due to the relatively short duration of the reaction at this temperature. At the end of the observation period at 400 °C, the fwhm[29] for the (004) peak is 0.149(1)°, and for the (103) peak is 0.230(1)°. These peaks are clearly broadened as compared to the end of the observation period at 450 °C, where the respective fwhm values are now 0.084(1)° and 0.097(1)°. The poor crystallinity makes it difficult to observe any potentially subtle change in the lattice parameters for $LaSrCoO_3H_y$ during the initial stage of formation.

However, the *c* parameter of the tetragonal phase is clearly decreasing with increasing time. The *c* parameter changes from an initial value of 13.222(9) Å to a final value of 13.181(3) Å at 400 °C.

Over the period of time in which measurements were collected at 400 °C the weight fraction of CaH_2 shows a decrease from 0.164(2) to 0.154(2), and that of CaO shows an increase from 0.099(3) to 0.109(3). A similarly small variation in this parameter is observed at 450 °C for these phases, with CaH_2 decreasing from 0.149(2) to 0.143(2) and CaO increasing from 0.116(3) to 0.124(3). These values compare with a room-temperature weight fraction of 0.314(2) for CaH_2 and zero for CaO, based upon Rietveld refinement of the room-temperature data. The room-temperature value of 0.314(2) is higher than the 0.21 expected from the 1:2.2 mole ratio of the starting materials, due to the much lower absorption of CaH_2 as compared with the cobaltate phases. However, it remains clear that a far greater decrease in the weight fraction of CaH_2 occurs during the formation of the $LaSrCoO_{3.5-x}$ phase (~85% of the total decrease) from $LaSrCoO_4$, than during the subsequent formation of $LaSrCoO_3H_y$ (~15% of the total decrease).

At 450 °C the *a* axes for both tetragonal oxide and orthorhombic oxide hydride phases were found to increase with time, while the variation in CaH_2 cell parameters indicates that the temperature could have decreased slightly (by approximately

(27) Bergsma, J.; Loopstra, B. O. *Acta Crystallogr.* **1962**, *15*, 92−93.
(28) Huang, Q.; Chmaissem, O.; Caponi, J. J.; Chaillout, C.; Marezio, M.; Tholence, J. L.; Santoro, A. *Physica C* **1994**, *227*, 1−9.

(29) To obtain these numbers for fwhm, the profile and $LaSrCoO_3H_y$ phase parameters were taken from a Rietveld refinement of the original data and were used to simulate a pattern. The simulated pattern was then fitted to obtain the reported numbers.

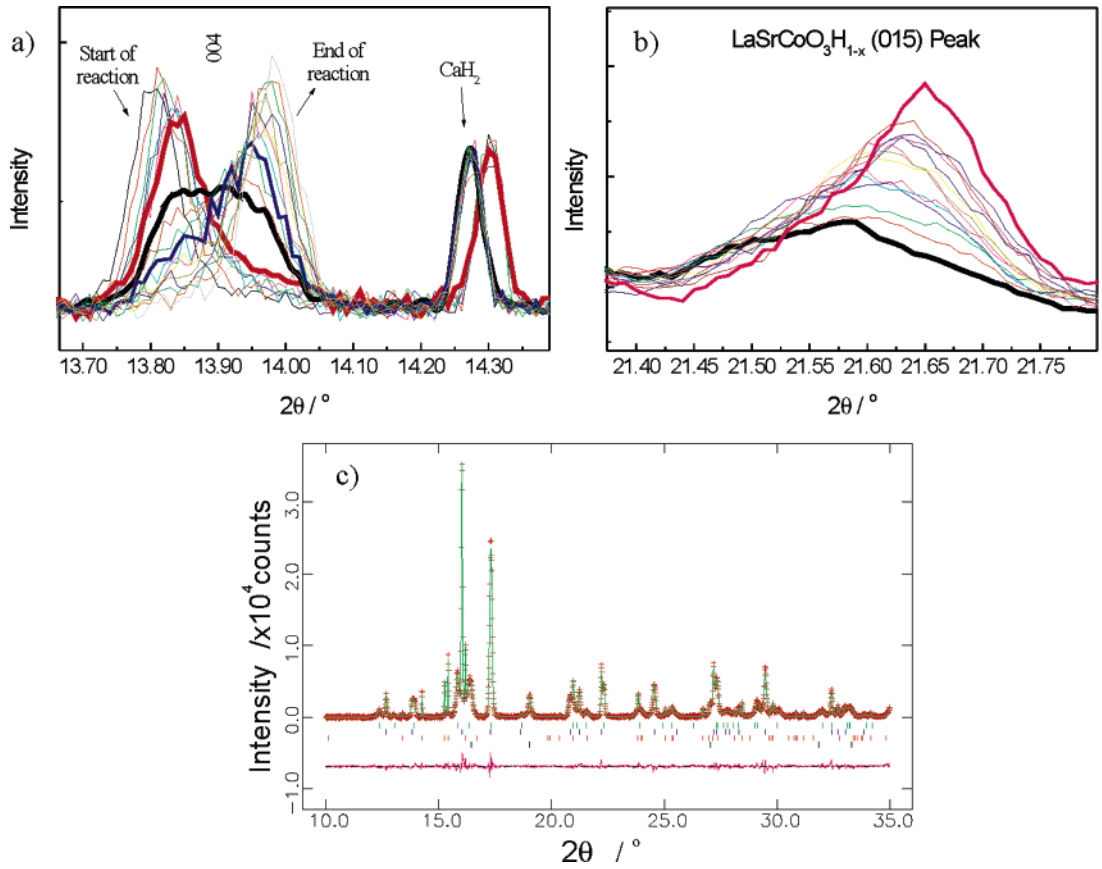

Figure 6. (a) Time-dependent variation of the (004) reflection during the reaction of $LaSrCoO_4$ and CaH_2 [1:2.2 mole ratio], which illustrates the gradual conversion of $LaSrCoO_{3.5-x}$ into $LaSrCoO_3H_y$. The thick red line indicates the final data set at 400 °C, and the thick black line, the first data set at 450 °C. (b) Smoothed 450 °C data illustrate the clear shift in peak position with time during the reaction, corresponding to the decrease in both the *c* and *b* axes of $LaSrCoO_3H_y$. In this plot the thick black line is the first data set, and the thick red line is the last data set. (c) Rietveld refinement of in situ X-ray diffraction data collected at Daresbury station 9.1. Phases present are indicated by the reflection markers and include from top to bottom: $LaSrCoO_3H_y$, $LaSrCoO_{3.5-x}$, CaH_2, and CaO. The first pattern collected during the reaction to form oxide hydride at 450 °C is shown. The figures of merit are $\chi^2 = 1.74$, $wR_p = 9.09\%$, $R_p = 6.95\%$.

10 °C)[30] during the data collection. This increase in cell parameter for the orthorhombic phase, while the reaction temperature is slowly decreasing, is not consistent with the temperature-dependent cell parameter evolution observed by powder neutron diffraction for $LaSrCoO_3H_{0.70(2)}$. This provides evidence that changes induced in the phases present by reaction, and not temperature variation, were the main factors in the change in cell constants with time at 450 °C. Furthermore, the fact that the *b* axis is decreasing while the *a* axis is increasing in the orthorhombic phase **1** *itself* demonstrates that the changes observed in the cell parameters as a function of time do not result from drift in the temperature during the reaction—both in-plane cell parameters increase with temperature on heating, and thus effects due solely to temperature variation cannot induce opposite variation of the two parameters. Plots of orthorhombic strain[31] in $LaSrCoO_3H_y$ versus time during the in situ reaction and of pure **1** with temperature are shown in Figure 8a.

The growth curve of $LaSrCoO_3H_y$ at 450 °C crosses the decay curve of the tetragonal reduced oxide phase at a weight fraction of 0.37, slightly over 50% of the maximum weight fraction attained by the oxide hydride (0.65). This conservation of the total scattering power as the reaction proceeds indicates that there is no intermediate conversion of some fraction of the material into an amorphous or very poorly crystalline phase during the reaction. The increase in the weight fraction of the orthorhombic phase has been fitted to the Avrami−Erofe'ev equation[32] (Figure 7b). An exponent of 1.10(7) has been determined, which is consistent with growth of **1** occurring in either one or two dimensions.

Accurate modeling of the diffraction profiles required inclusion of anisotropic broadening of the $LaSrCoO_{3.5-x}$ and $LaSrCoO_3H_y$ peak shapes which was refined using the Stephens model of microstrain broadening,[33] as implemented in GSAS. In this model, strain broadening is a result of each crystallite having its own set of lattice parameters. The mean distribution of lattice parameters in the sample follows the symmetry of the crystal structure, although individual grains may not follow this symmetry. Starting from the expression for the d-spacing of a reflection,

$$\frac{1}{d^2} = M_{hkl} = Ah^2 + Bk^2 + Cl^2 + Dkl + Ehl + Fhk \quad (1)$$

where $\{A, ..., F\}$ are metric parameters of the reciprocal lattice,

(30) This result has been determined on the basis of an estimate of the thermal expansion of CaH_2, obtained from in situ XRD data collected in this study.
(31) Defined as strain $= 2(a - b)/(a + b)$.
(32) Avrami, M. *J. Chem. Phys.* **1941**, *9*, 177.
(33) Stephens, P. W. *J. Appl. Cryst.* **1999**, *32*, 281−289.

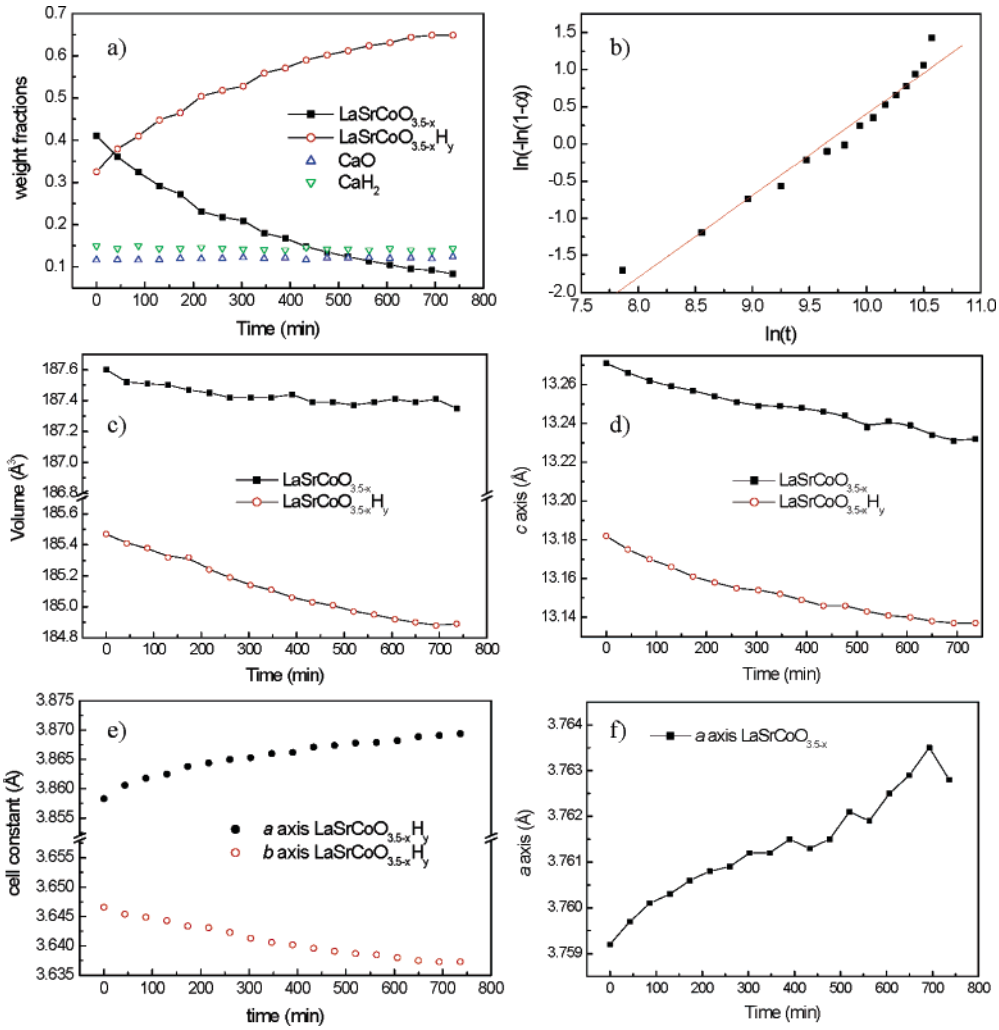

Figure 7. (a) Time-dependent variation of weight fractions during the reaction of $LaSrCoO_4$ and CaH_2 [1:2.2 mole ratio] at 450 °C. The phases present include $LaSrCoO_{3.5-x}$, $LaSrCoO_3H_y$, CaO, and CaH_2. (b) Fit of normalized weight fraction data for $LaSrCoO_3H_y$ to the Avrami−Erofe'ev equation. (c) Variation in the unit cell volumes versus time for $LaSrCoO_{3.5-x}$ and $LaSrCoO_3H_y$ (d−f) Variation in the cell constants versus time for $LaSrCoO_{3.5-x}$ and $LaSrCoO_3H_y$ during the reaction at 450 °C. For these figures the error of each data point is less than the size of the symbol that represents it.

an expression for the microstrain broadening (the variance of M_{hkl}) is

$$\sigma^2(M_{hkl}) = \sum_{HKL} S_{HKL} h^H k^K l^L \qquad (2)$$

In eq 2, the terms S_{HKL} are defined for $H + K + L = 4$. The model is further expanded by Stephens to include both Gaussian and Lorentzian contributions to the anisotropic broadening, as implemented in GSAS. To illustrate the application of eq 2, we may consider that the only anisotropic contribution to the width of the 00*l* peaks in $LaSrCoO_3H_y$ is from the S_{004} term. However, the (0*kl*) peaks contain contributions from the S_{040}, S_{004}, and S_{022} terms.

In the case of orthorhombic $LaSrCoO_3H_y$, symmetry arguments reduce the number of possible S_{HKL} parameters from 15 to 6: S_{400}, S_{040}, S_{202}, S_{022}, S_{004}, and S_{220}. As the S_{004} term for strain broadening of the 00*l* reflections was found to be negligibly small, it was set to zero for the final stage of the refinements. The results indicate that strain broadening is dominated by the Gaussian component during the formation of **1** (the mixing factor ϵ diverged when refined and was thus held at zero). The time dependence of the S_{HKL} anisotropic broadening parameters for the oxide hydride **1** at 450 °C is presented in Figure 9, which shows the overall decrease in anisotropy as the reaction proceeds.

The results from capillary 1 have been compared with those of six other capillaries. For a 1:1 mixture of $LaSrCoO_4$ and CaH_2 (capillary 2), the $LaSrCoO_{3.5-x}$ phase visibly forms near a temperature of 250 °C, although peaks from the $LaSrCoO_4$ phase begin to decrease in intensity above 125 °C. This observation is confirmed by studies on five other capillaries containing a 1:2.2 mole ratio of $LaSrCoO_4$ to CaH_2 (capillaries 3−7).[34] These additional capillaries were heated to temperatures ranging from 450 to 570 °C, and in each of these experiments the oxygen deficient $LaSrCoO_{3.5-x}$ phase is formed during heating.

Other aspects of the in situ reaction were found to be capillary dependent. During the in situ study of capillary 3, only weak peaks of the orthorhombic oxide hydride were observed along with a majority $LaSrCoO_{3.5-x}$ phase at 450 °C. The weak peaks from $LaSrCoO_3H_y$ were not present in diffraction patterns collected at 500 °C, suggesting that under the conditions present in this capillary the phase is not stable at this temperature. This

(34) Details of the temperature programs for capillaries 3−7 are given in the Supporting Information.

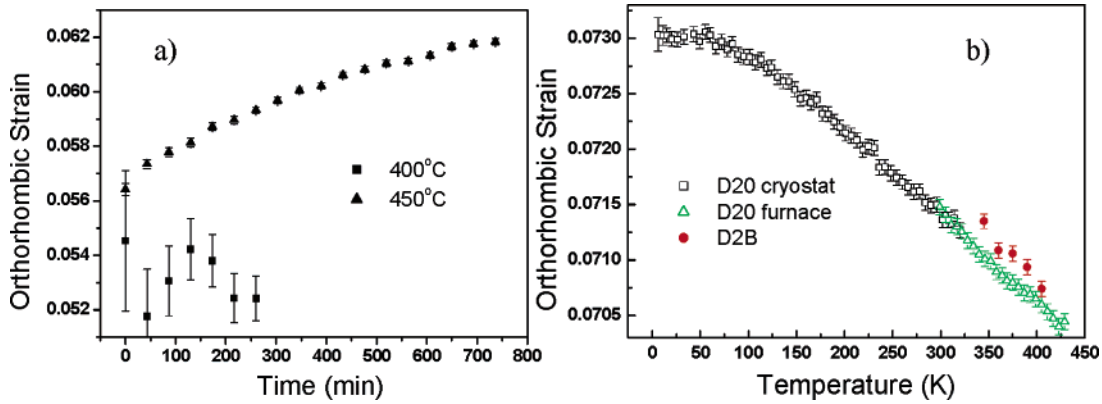

Figure 8. (a) Time-dependent variation of orthorhombic strain during the reaction of $LaSrCoO_4$ and CaH_2 [1:2.2 mole ratio] at 400 and 450 °C. (b) Temperature-dependent variation of orthorhombic strain for $LaSrCoO_3H_{0.70(2)}$.

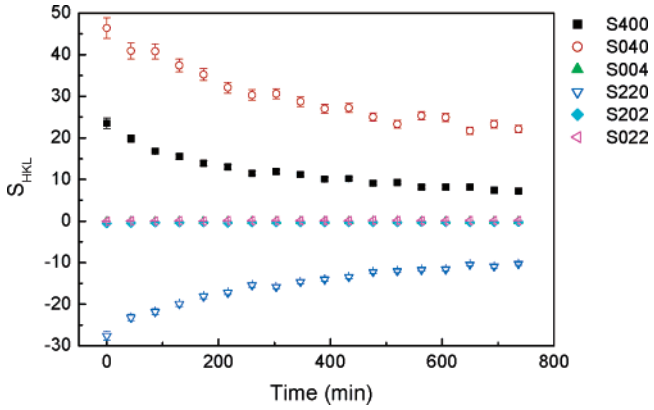

Figure 9. Comparison of the six symmetry-allowed anisotropic broadening terms obtained from Rietveld refinement of $LaSrCoO_3H_y$. The data refined were in situ powder X-ray diffraction patterns obtained at 450 °C.

contrasts with the apparent stability of the phase at 500 °C in capillary 1. During the study of capillary 4 the $LaSrCoO_{3.5-x}$ phase was formed, but no evidence was found for $LaSrCoO_3H_y$ up to 570 °C. Significant quantities of $LaSrCoO_3H_y$ were formed in capillaries 5 and 6, while in capillary 7 the reaction to form **1** went to completion in 4 h at 450 °C. The various results can be reconciled if the capillaries were poorly mixed or had become somewhat segregated due to the agitation required to fill the capillaries. Eliminating the excess CaH_2 had a similar result, as a 1:1 mixture of reagents (capillary 2) was found to form $LaSrCoO_{3.5-x}$ but not **1**.[35] These results highlight the importance of physical contact between the reagents for the formation of the oxide hydride.

The in situ data directly led one to consider comparing the observed tetragonal intermediate phase with other reduced $LaSrCoO_4$ phases. To investigate this comparison, synchrotron XRD data were collected at room temperature on sample B (340 °C for 15 h). The capillary contained a mixture of the $LaSrCoO_{3.5-x}$- and $LaSrCoO_3H_y$-type phases, CaH_2, and CaO after quenching. The distribution of cobaltate phases was refined as 36(1)% $LaSrCoO_3H_y$ and 64(1)% $LaSrCoO_{3.5-x}$ by weight. Cell constants obtained from Rietveld refinement of these data are shown along with data from previous studies in Table 1. The volume of the cell increases from $LaSrCoO_4$ to $LaSrCoO_{3.5\pm\delta}$, but *decreases* again to form $LaSrCoO_3H_y$, the volume of which is similar to that of $LaSrCoO_4$. This decrease in volume is mainly due to the decrease in the *c* parameter, as the *a* parameter is *higher* in the CaH_2-reduced $LaSrCoO_{3.5-x}$-type phase than in that of the $LaSrCoO_{3.38(2)}$-type phase. This increase in the *a* axis, in conjunction with a decrease in the *c* axis, reproduces the trend observed at 450 °C while following the reaction by in situ XRD. The trends in cell parameters suggest that the tetragonal **2** phases formed by high-temperature reduction with CaH_2 are qualitatively different than those reported in the literature.[9]

The successful formation of oxide hydride from $LaSrCoO_{3.5-x}$ starting material (which does not contain the hydride anion) is demonstrated by sample C. This sample contained a mixture of $LaSrCoO_3H_y$:$LaSrCoO_{3.5-x}$ in the mass ratio 61(2):39(2). As observed for sample B above, the cell constants suggest that the reduced oxide in C corresponds to a qualitatively different phase than has been reported in the literature.[9]

The stability of washed **1** was examined by annealing at the reaction temperature in a sealed evacuated tube (sample D). The cell constants of sample D are very close to those of nonannealed samples (Table 1), indicating that the washed material does not decompose upon annealing at the reaction conditions. D was of further use in examining the effect of annealing on the width of the peaks. A comparison between the fwhm of various reflections is given in Table S13 for sample D before washing and annealing (nonannealed) and after the washing and annealing stage. It is interesting to note that in contrast to the in situ results, the fwhm of the 110 reflection is significantly larger than that of 004 in both annealed and nonannealed material. Examination of all of the reflections in the nonannealed sample reveals that over the 48 h the sample has reacted, the anisotropy in reflections for which *k* is zero has decreased much more than those with nonzero *k* indices. The distribution of distances along the *b* axis in the nonannealed sample is such that peaks with nonzero *k* indices are extremely difficult to fit, as shown in Figure S14. After annealing, the peaks have sharpened considerably, making it possible to fit the 011, 013, and 110 reflections with a single-phase model.

The influence of reaction ramp rate and sample loading was tested in the series of samples E−H. Samples E and G contained 0.05 g of reaction mixture which corresponds to 0.7 bar of hydrogen pressure generated in the tube[36] and were ramped at different rates, but in both cases only very weak peaks attributed to the oxide hydride were present. However, in samples F and

(35) Ex situ experiments on sample J produced a mixture of oxide hydride and $LaSrCoO_{3.5-x}$, indicating that oxide hydride may be formed with a ratio of $LaSrCoO_4$:CaH_2 less than 1:2.

Table 1. Room-Temperature Data For Reduced Cobaltates Derived From $LaSrCoO_4$

	a (Å)	b (Å)	d_{110} (Å)	c (Å)	V (Å^3)
$LaSrCoO_4$	3.8052(3)	−	2.6907(2)	12.540(1)	181.57(4)
$LaSrCoO_{3.57(1)}$[a]	3.74636(8)	−	2.64908(6)	13.3201(2)	186.95(1)
$LaSrCoO_{3.432(8)}$[a]	3.74544(8)	−	2.64843(6)	13.3408(2)	187.14(1)
$LaSrCoO_{3.38(2)}$[b]	3.7419(1)	−	2.6459(1)	13.2712(5)	185.82(2)
$LaSrCoO_{3.5-x}$[c]	3.7446(1)	−	2.6478(1)	13.1838(3)	184.864(5)
$LaSrCoO_{3.5-x}$[d]	3.7529(8)	−	2.6537(6)	13.161(3)	185.37(9)
$LaSrCoO_{3.5-x}$[e]	3.7559(1)	−	2.6558(1)	13.1562(5)	185.586(5)
$LaSrCoO_3H_{0.70(2)}$[f]	3.8711(1)	3.6032(1)	2.6375(1)	13.0177(1)	181.58(1)
$LaSrCoO_3H_x$[g]	3.8701(1)	3.6086(1)	2.6393(1)	13.0122(3)	181.73(1)

[a] Reaction of $LaSrCoO_4$ and 8%H_2/98%N_2 at 550 °C for 4 h.[9] [b] Reaction of $LaSrCoO_4$ and NaH [1:2] at 200 °C for 12 days.[9] [c] Quenched from a reaction of $LaSrCoO_4$ and CaH_2 [1:2.2] at 340 °C for 15 h (sample B). [d] Reaction of $LaSrCoO_{3.5-x}$ and CaH_2 [1:2.2] at 450 °C for 12 h (sample C). [e] Reaction of $LaSrCoO_4$ and CaH_2 [1:1.05] at 450 °C for 48 h (sample J). [f] From ref 10, a reaction between $LaSrCoO_4$ and CaH_2 [1:2] at 450 °C for 48 h (sample A). [g] Annealed oxide hydride (sample D).

H (0.8 g of reaction mixture, 11 bar hydrogen pressure in the tube at reaction temperature) the $LaSrCoO_{3.5-x}$ phase reacted completely to form $LaSrCoO_3H_y$. Therefore, the ramp rate does not influence the formation of $LaSrCoO_3H_y$, but the pressure of H_2 gas formed in the reaction vessel (due to the formation of CaO when CaH_2 acts as a reducing reagent in these reactions) has an impact on the formation of oxide hydride as opposed to reduced oxide phases.

The effect of hydrogen pressure was further examined by reacting a mixture of $LaSrCoO_4$ and CaH_2 under dynamic vacuum (sample I). The H_2 formed during the reduction of $LaSrCoO_4$ is immediately removed from the environment of the sample. X-ray diffraction data indicate that the product of this reaction was mainly $LaSrCoO_{3.5-x}$, although approximately one-third of the cobaltate material consisted of slightly reduced oxide of general composition $LaSrCoO_{4-x}$, along with CaO and CaH_2.[37] There was no evidence for the presence of oxide hydride phases. The fact that the starting material was not completely reduced in sample I after 15 h at 450 °C in comparison with reduction in a sealed capillary for 15 h at 340 °C to a mixture of the $LaSrCoO_{3.5-x}$- and $LaSrCoO_3H_y$-type phases (sample B), suggests that the reduction to $LaSrCoO_{3.5-x}$ is also influenced by the pressure of H_2.

Thermogravimetric oxidation data were obtained on sample J in combination with a mass spectroscopic analysis of evolved H_2O. Rietveld refinement of laboratory X-ray diffraction data indicated that this sample contained a mixture of $LaSrCoO_3H_y$: $LaSrCoO_{3.5-x}$ in the mass ratio 62(1):38(1). As observed for sample B and C above, the cell constants suggest that J differs from the reduced oxide phases reported in ref 9.[9] The oxidation of oxide hydride material above ~200 °C produced a visible peak of H_2O. The quantity of H_2O indicates that the hydride anion is present in the sample at a level of ~0.3 mol per mole of lanthanum strontium cobaltate material. This is significantly less than the composition of $LaSrCoO_3H_{0.7}$ expected in the final product. However, this would correspond to ~0.5 mol of hydride per mole of the orthorhombic phase, which is much closer to the level expected in **1**. In summary, the TGA data suggest that the incompletely reacted material contains less hydride anion than the $LaSrCoO_3H_{0.7}$ final product.

Discussion

The unusual coexistence of oxide and hydride anions with a divalent transition metal cation produces questions about the electronic properties and electronic structure of the material which we address here by combining experimental information about the strength of the interactions between the cobalt centers through determination of the three-dimensional magnetic ordering temperature with calculation of the electronic structure. The introduction of the hydride anion into the oxide array must occur by a kinetically controlled pathway which avoids complete reduction to the metal—as examples of transition metal oxide hydrides are rare, the identification of the pathway for the formation of **1** is important, as the ability to form the phases required en route to **1** may be a chemical prerequisite for other compositions to act as precursors to transition metal oxide hydride formation in a manner similar to that of $LaSrCoO_4$.

The electronic structure calculations are presented here with the aim of contrasting the bonding in the oxide hydride with that in transition metal oxides, where the importance of metal-oxide covalency in controlling electronic properties such as localization versus delocalization and magnetic exchange are well-known. While other examples of well-characterized oxide hydrides (LaHO,[12] $Ba_3(AlO_4)H$,[38] $Ba_{21}Ge_2O_5H_{24}$[11]) have been reported, to our knowledge no computational studies have been reported on these compounds.

The differences observed in the electronic structures of the three possible representations of the La/Sr substitutional disorder only effect interactions within the rocksalt layer and are shown quantitatively to have only a minor influence on the contribution to the electronic structure of the orbital overlap within the CoOH layer, which is the main focus of the paper. The *Imm*2 structure is expected to give a closer approximation to the random La^{3+}/Sr^{2+} distribution found in the *Immm* structure, than would the *Pmm*2 results. The *Imm*2 structure is preferred as all anions are coordinated to a mixture of La^{3+} and Sr^{2+}, in contrast to the second and third distributions of *Pmm*2, and hence the electronic structure of **1** is discussed using these results.

The partial DOS indicate a close relationship between the occurrence of Co $3d_{x^2-y^2}$ and H 1s states in the electronic structure, reflecting covalent overlap of the type shown in Figure S3. This mixing of Co 3d, H 1s, and O2 2p states within the

(36) The estimates of pressure are based on the assumption that the maximum possible pressure would involve decomposition of 1 mol equiv of CaH_2 to Ca metal and H_2 gas. Masses refer to a mixture of $LaSrCoO_4$ and CaH_2 at a molar ratio of 1:2.

(37) The slightly reduced portion of the product labeled $LaSrCoO_{4-x}$ has been identified on the basis of its lattice parameters, which are intermediate between those of $LaSrCoO_4$ and $LaSrCoO_{3.5}$. The extremely broad nature of the reflections indicates that this material contains a range of oxygen content, indicating a solid solution rather than a stoichiometric intermediate phase.

(38) Huang, B. Q.; Corbett, J. D. *J. Solid State Chem* **1998**, *141*, 570−575.

perovskite layer is further confirmed by the atomic parentage of the band states in Figure 4. The mixing of 3d and 1s orbitals is significant due to the link between these orbitals and the electronic properties of the material.

FPLAPW calculations have been carried out on $LaSrCoO_4$ to provide a basis for understanding the influence of hydrogen on the electronic structure of $LaSrCoO_3H$. The similarity of the electronic structures of the two materials (oxide and oxide hydride) indicates that the H 1s orbital in **1** can be thought of as substituting for the O4 $2p_y$ orbital in $LaSrCoO_4$ into electronic states arising from σ bonding overlap between metal x^2-y^2 and in-plane anion states. (Figure 3d−f). The bands in the region below −4.6 eV exhibit strong contributions from mixing that occurs within the $CoO_{2-x}H_x$ layer. In addition, mixing with higher-energy orbitals produces a significant H 1s DOS in **1** well above the Fermi energy, although the majority of hydrogen states are situated near the bottom of the valence band. The existence of H 1s states at such high energies, as is observed for the O4 states of $LaSrCoO_4$ (Figure 3e), reflects the interactions with metal orbitals and is further evidence of covalent interactions that play an important role in the electronic properties of **1**. The similarity in the distribution of H 1s and O4 states indicates that the hydride anion can play a similar role to that of oxide in controlling the electronic properties of **1**. This is reflected in the comparison of total O4 and H 1s states in Figure 3e. The enhanced width of the Co $3d_{x^2-y^2}$ states in **1** indicates that overlap of this key metal orbital with both oxide and hydride is greater in this material than in $LaSrCoO_4$, providing an important qualitative link with the high magnetic ordering temperature of **1** compared with pure Co oxide analogues—the Co bandwidth directly reflects the spreading in energy of the Co d states due to mixing with the states of neighboring anions. The enhanced contribution of the x^2-y^2 compared with z^2 Co 3d state at lower energies also reflects the interaction between the in-plane orbitals of metal and anions.

It is worthwhile to further compare the Co−H mixing in $LaSrCoO_3H$ with that in pure hydrides of the transition metals. The rocksalt structure binary hydrides of the transition metals have been examined using ab initio DFT calculations.[39,40] The hydride 1s states of CoH are mainly situated in the range of −6 to −7.5 eV below the Fermi energy, although due to the presence of a free electron tail, the full width of the H 1s DOS in this energy region is approximately 5.7 eV.[39] Furthermore, mixing of Co e_g states into the lower-energy H 1s states was found, due to the direct overlap of these orbitals in the rocksalt structure. This is analogous to the metal 3d−hydride 1s mixing in $LaSrCoO_3H$, which produces a DOS for H 1s largely distributed over the valence band (5.4 eV wide), while also providing small contributions to the H 1s DOS in the conduction band and above the Fermi level. The Co−H distances in the fcc CoH structure are remarkably similar to those in the oxide hydride: 1.80 Å in the fully relaxed fcc CoH structure based upon LDA calculations, 1.87 Å from experimental data on fcc CoH,[39,40] and 1.80174(2) Å for **1** at room temperature. On the basis of these distances, the extent of overlap between metal and hydride orbitals may be expected to be similar in the two materials, as appears to be the case from the detailed comparison of densities of states. These results provide important theoretical and experimental links between the oxide-containing hydrides and the rather covalent binary transition metal hydrides. The Co−H bond lengths and bandwidths of the 1s states in both cases are similar, although the properties of the Co-derived electrons in **1** are controlled also by interaction with oxide, producing the magnetic insulating behavior observed.

The electronic structures of the more ionic binary alkali and alkaline earth hydrides provide an important contrast to the covalent interactions found in **1** and the transition metal hydrides. KH also crystallizes in the rocksalt structure. The lower-energy hydride states are now filled, with the Fermi energy situated at the top of the valence band.[39] The valence band is now very sharp (a width of ∼2.3 eV in KH as compared with ∼5.4 eV for the H states in **1**, and ∼5.7 eV for the H states in CoH), with the states having almost exclusively H 1s character. Only an extremely small contribution from these states is observed at higher energies. The absence of a metal contribution to the low-energy region of the electronic structure and the concentration of H 1s states to a narrow energy range rather than bonding-induced contributions over the entire valence region, as found in **1**, are thus characteristic of ionic hydride electronic structure. The mixing of the H 1s state with the metal orbitals and the resulting distribution of H 1s character over the electronic structure in oxide hydride **1** are qualitatively more consistent with those of the transition metal hydrides than the alkali hydrides, suggesting that the presence of H will make a direct contribution to the electronic properties by modulating the interaction between the cobalt centers. Together with the comparison with the electronic structure of the $LaSrCoO_4$ starting material, this allows one to conclude that both the oxide and hydride frontier orbitals are involved in mediating electronic communication between the metal centers. Analogy with the covalent interaction between metal and oxide, which is well-established as producing superexchange interactions in pure transition metal oxides, then indicates that metal-hydride mixing should contribute to the superexchange paths contributing to the electronic structure of the material. The σ H−Co−H interactions provide an important pathway for magnetic exchange to occur, impacting strongly on the high-temperature long-range ordering reported in this contribution.

The neutron diffraction data demonstrate experimentally the existence of strong superexchange interactions between the transition metal cations in **1**, producing an antiferromagnetically ordered ground state. The observed magnetic ordering temperature of 380 K points to the strength of the superexchange interactions between the cobalt cations. The cobalt centers are sufficiently separated in this material that the dominant magnetic interactions are via a superexchange mechanism. The ordering temperature indicates that Co−H−Co superexchange, exclusively through the σ orbital interactions examined in the DFT study, are very strong. This can be judged by comparison with the Neel temperature of oxides adopting the single-layer K_2NiF_4 structure, which are 270 K for La_2CoO_4,[41] ∼330 K for La_2NiO_4[42] and ∼320 K for La_2CuO_4.[43] This similar but elevated ordering temperature fits with the idea that the electronic

(39) Smithson, H.; Marianetti, C. A.; Morgan, D.; de Ven, A. V.; Predith, A.; Ceder, G. *Phys. Rev. B* **2002**, *66*, 144107−144116.
(40) Singh, D. J.; Papaconstantopoulos, D. A. *Phys. Rev. B* **1994**, *49*, 12801−12804.
(41) Furukawa, Y.; Wada, S.; Kajitani, T.; Hosoya, S. *J. Phys. Soc. Jpn.* **1999**, *68*, 346−349.
(42) Castro, M.; Burriel, R. *Thermochim. Acta* **1995**, *269/270*, 537−552.
(43) MacLaughlin, D. E.; Vithayathil, J. P.; Brom, H. B.; de Rooy, J. C. J. M.; Hammel, P. C.; Canfield, P. C.; Reyes, A. P.; Fisk, Z.; Thompson, J. D.; Cheong, S.-W. *Phys. Rev. Lett.* **1994**, *72*, 760−763.

structure is similar to that of the pure oxide $LaSrCoO_4$ with the in-plane states coming from the O4 $2p_y$ orbital replaced effectively by the H 1s states—experiment reveals that the H states are actually more effective in transmitting electronic interactions than the oxide states they replace. The two-dimensional nature of the material means that the enhanced three-dimensional ordering temperature cannot be directly attributed to the difference between oxide- and hydride-mediated superexchange. In a layered material, the onset of three-dimensional order is controlled by the interlayer coupling J', although strong intralayer coupling leads to short-range order characterized by a correlation length ξ within the plane which enhances T_N over that expected due solely to the interplane coupling according to eq 3

$$kT_N = \left(\frac{\xi}{a}\right)^2 J'S^2 \qquad (3)$$

where a is the separation between magnetic centers in the plane. The detailed outcome of the calculations is consistent with the cobalt-hydride coupling being at least as strong as the cobalt-oxide interaction, and thus consistent with the enhanced ordering temperature of **1** being associated with stronger in-plane superexchange interactions. Interestingly, the σ-only character of the frontier orbitals of the hydride anion would be expected to produce purely antiferromagnetic superexchange between the half-filled e_g orbitals of two adjacent cobalt cations with only weaker direct exchange interactions between the π symmetry t_{2g} states. The oxide anion-mediated σ-exchange pathway is in competition with the π-exchange which is formally an interaction between a single hole in each t_{2g} state. This would be expected to be ferromagnetic and thus compete with the σ- interaction and weaken the overall antiferromagnetic superexchange. The frontier orbital symmetry of the hydride anion is thus consistent with the higher observed antiferromagnetic ordering temperature compared with that of the oxide anions.

The expected staggered moment for contributions from a fully ordered 70% high spin (HS) Co(II) ($S = {}^3/_2$) and 30% HS Co(I) ($S = 1$), based upon the composition $LaSrCoO_3H_{0.70(2)}$ obtained from combined X-ray and neutron diffraction refinements in the earlier study, is 2.7 μ_B. The refined moment corresponds to a mixture of 76% HS Co(II) and 24% HS Co (I), for an average oxidation state of $Co^{1.76+}$. The refined hydride content for all data presented in this report, obtained on both D20 and D2B, agree within error to a value of 0.57(1)[44] with an expected moment of 2.57μ_B. The discrepancy may reflect the difficulty in obtaining a precise value for the hydride content by powder neutron diffraction. It is important to note that the neutron data define only the mean scattering length on the hydride site (which is negative due to the sign of the H scattering length), so a higher H content together with O occupancy can equally fit the data. Assuming full occupancy by combined hydride and oxide gives $LaSrCoO_{3.171(4)}H_{0.829(4)}$, which corresponds to $Co^{2.171+}$ (82.9% Co(II) and 17.1% Co(III)), and an expected moment of 2.49μ_B. This possibility is rejected as it would require the $LaSrCoO_{3.5}$ intermediate (vide infra) in the pathway leading to **1** to be oxidized by CaH_2 to form **1**. However the composition $LaSrCoO_{3.056(7)}H_{0.65}$ fits both the refined staggered moment and the observed negative scattering density. In view of the reduction in staggered moment expected due both to covalency and disorder, we will use the originally refined $H_{0.7}$ composition in discussing the properties of **1** in the remainder of the report.

The effective replacement of the 2p states of the oxide anion substituted by hydride to form **1** by the H 1s states reflects the structural replacement of oxide by hydride in the reaction to form $LaSrCoO_3H_{0.7}$ from $LaSrCoO_4$. This involves substitution of oxide by hydride and occurs at relatively low temperatures for processes involving solids. The identification of the phases involved in the transformation can both shed light on the mechanism by which the substitution occurs and identify the characteristic chemical features of the $LaSrCoO_4$ system which allow the formation of the unusual oxide hydride to take place—as the process is kinetically controlled, the ability to access the phases in the pathway to **1** are critical to the ability to form **1** at all. The limiting mechanisms possible are substitution of hydride for oxide directly and removal of oxide followed by insertion of hydrogen. Clearly diffraction measurements are unable to precisely identify the microscopic atomic processes involved in the transformation in detail, but the identification of the phases involved and some details of their structures can place limits on the atomic motions that can be proposed to occur during the transformation.

The reduction products of $LaSrCoO_{4-x}$ depend critically upon the reagents and reaction temperatures. At elevated temperatures ($>\sim$350 °C) and one atmosphere of H_2 the limiting composition formed before complete reduction to cobalt metal is $LaSrCoO_{3.5}$.[9] Lower-temperature reaction (200 °C) with NaH stabilized the more reduced phase $LaSrCoO_{3.38(2)}$.[9] Ex situ studies have previously shown that $LaSrCoO_4$ reacts with CaH_2 at 450 °C for 2 periods of 4 days to form $LaSrCoO_3H_{0.70(2)}$.[10] In this work, every in situ study leading to the formation of **1** involved formation of a tetragonal reduced oxide (hereinafter referred to as **2** to reflect the possibility that the material formed in situ is not identical to the phases previously isolated and studied at room temperature) and this phase may therefore be considered a necessary intermediate phase in the formation of the oxide hydride. There is no evidence for formation of **1** without prior formation of **2**. In the study of capillary 1, formation of tetragonal **2** is then followed by transformation into orthorhombic oxide hydride **1** which occurs slowly (and with poorly crystalline **1**) at 400 °C and more rapidly at 450 °C. The detailed Rietveld analyses of this transformation reveal that this apparently simple reaction is actually complicated because during formation of the oxide hydride the structures of both **1** and **2** are evolving, both in terms of the mean crystal structures over a distance scale of several hundred angstroms (judged by the cell parameters) and the distribution of these structures about the mean over shorter distances as judged by the anisotropic broadening of the Bragg reflections.

The smooth increase in orthorhombic distortion of **1** with reaction time in the in situ runs is evidence for increasing hydride concentration and/or oxide/hydride site order in **1**, and suggests that intermediate oxide hydride phases (differing either in composition or oxide/hydride site order) exist between the compositions $LaSrCoO_{3.5}$ and $LaSrCoO_3H_{0.7}$. The difference in orthorhombic strain of **1** between 400 and 450 °C is particularly striking in this regard—at equilibrium the orthorhombic strain decreases with increasing temperature (Figure 8b) so the

(44) This value of hydride content was obtained from a fit to the 6 K neutron diffraction data obtained on D20.

Scheme 1. Formation Pathway for **1**

$$LaSrCoO_4 + CaH_2 \xrightarrow{a} LaSrCoO_{3.38-x}\ (\mathbf{2}) + (0.38\text{-}x)CaH_2 + (0.62+x)CaO + (0.62+x)H_2$$

$$\xrightarrow{b} LaSrCoO_{3.38-x}H_y\ (\mathbf{2}\ \text{tetragonal}) + LaSrCoO_3H_z\ (\mathbf{1}\ \text{orthorhombic}) + (0.38\text{-}x)CaH_2 +$$

$$(0.62+x)CaO + (0.62+x\text{-}y/2\text{-}z/2)H_2 \xrightarrow{c} LaSrCoO_3H_{0.7}\ (\text{orthorhombic}) + CaO + 0.65\ H_2$$

increased strain in **1** on heating from 400 to 450 °C and on continued reaction at 450 °C is a kinetic effect reflecting the details of the formation of **1**. This must be accounted for together with other defining observations which include the initially rapid then finally slow evolution of CaH_2 and CaO phase fractions, the TG−MS demonstration that hydride incorporation into the reaction mixture increases with increasing conversion from tetragonal to orthorhombic, the differing unit cell volumes of **1** and **2** which indicate these phases have different compositions, and the roles of mixing and gaseous hydrogen.

Direct hydride substitution for oxide coupled with reduction to form **1** directly from $LaSrCoO_4$ is excluded by the observation of the intermediate phase **2**. The evolution of both tetragonal **2** and orthorhombic **1** with time indicates a range of intervening structures for both phases. We can identify two limiting cases which require an intermediate phase.

(i) Over-reduction to form a heavily reduced oxide with a lower formal Co oxidation state than **1** e.g. the putative Co(I) phase $LaSrCoO_3$ from which all oxygen required for the final transformation from $LaSrCoO_4$ to **1** is removed but no H is inserted: this gives the final phase fractions of CaH_2 and CaO early in the reaction and "stores" the required hydrogen as gaseous H_2. **1** is then formed by oxidation of $LaSrCoO_3$ by H_2(g) in a second slower step. This mechanism can be ruled out because the formation of heavily reduced $LaSrCoO_3$ would give a much smaller volume for **2** than is observed ($LaSrNiO_3$ has a unit cell volume of 176.8 Å^3 and is also orthorhombic due to vacancy ordering). Both in situ and ex situ data require the composition of **2** to be closer to $LaSrCoO_{3.38}$ than this mechanism requires.

(ii) Initial fast formation of a reduced oxide **2** with a Co oxidation state similar to that in **1** followed by a slow step in which two hydride anions from CaH_2 substitute for one oxide anion and the structure relaxes from tetragonal to orthorhombic. This allows the structure of **2** to evolve during the formation of **1**, as it can incorporate a small amount of hydride or change further in oxygen content as the reaction proceeds—we can write **2** as $LaSrCoO_{3+x}H_y$ where $0 \leq x < 0.38$, reflecting both the cell volumes of **2** in in situ and quenched ex situ reactions and the likelihood that the more forcing temperature conditions will produce a higher anion vacancy content than found for material formed at 200 °C with NaH. The hydrogen content y in **2** is lower than a limiting value y_{max}, reflecting the likelihood that high hydride concentrations can only be accommodated in orthorhombic oxide/hydride ordered structures. Both x and y in **2** vary with time. **1** is written as $LaSrCoO_3H_z$, where $y_{max} < z < 0.7$ and evolves in structure with time as z increases (as directly demonstrated by the TG−MS data on J) and the O/H order evolves within the xy plane. This can be directly inferred from the refined macro- and microstrains as hydrogen is initially delivered equivalently along the x and y axes of **2**. This pathway is outlined in Scheme 1.

The reduction step a is thus faster than the substitution step b which involves both oxide and hydride diffusion through the solid and then subsequent rearrangement from orthorhombic to tetragonal. a can be directly related to the initial rapid variation in CaH_2- and CaO-phase fractions where the pure reduction to $LaSrCoO_{3.38}$ followed by substitution to form $LaSrCoO_3H_{0.7}$ requires 62% of CaO to be formed in the initial step—given the absolute errors due to absorption giving an overestimate of the refined CaO fraction, this is consistent with the observation of 80% CaO formation in the first 43 min. The second step b is slower as both oxide and hydride diffusion and the local reorganization indicated by the anisotropic microstrain are involved. The incorporation of a critical H concentration into **2** triggers the formation of orthorhombic **1** in which the hydrogen content is sufficient to force a distinction between the x and y directions, with residual O/H disorder from the tetragonal precursor (as H is initially introduced with equally probability along x and y in the plane) removed as the reaction proceeds.

The solid hydride CaH_2 reagent is clearly essential for the formation of oxide hydride **1** which does not form with H_2 gas alone. The importance of mixing is also consistent with the predominantly solid−solid nature of both steps. The mechanism allows gas-phase H_2 to play an important role, consistent with the observation that the removal of hydrogen under dynamic vacuum drastically slows even the formation of reduced oxide. H_2 may be involved catalytically (e.g. in forming Co nanoparticles that then activate gas-phase H_2 to insertion into the solid or in maintaining a clean surface for the solid−solid reactions a and b to proceed on the complex oxide particles) and also the H_2 pressure generated in a sealed system may be vital for the equilibrium stability of **1** with respect to hydrogen loss under reaction conditions. CaH_2 is required to reduce Co within the K_2NiF_4 oxide structure to a lower oxidation state than possible with H_2 alone—this tetragonal intermediate **2** can then acquire hydride anions by both oxidation by gaseous H_2 or by substitution by hydride for oxide (step b).

The macroscopic evolution of the structure as tetragonal reduced oxide is transformed into orthorhombic oxide hydride is also reflected in the evolution of the microstrain broadening of the Bragg reflections in **1** as the reaction proceeds. The individual S_{HKL} terms provide a basis for examining the variation in broadening as the reaction proceeds. The relationship between these terms and the broadening of individual reflections is described in (2). The anisotropic broadening was particularly pronounced during the initial formation of the oxide hydride **1**, decreasing as the reaction proceeded. In all diffraction patterns the magnitude of the S_{400} and S_{040} parameters for $LaSrCoO_3H_{0.7}$ for this phase were strongly positive, the S_{004} parameter was negligible (indicating insignificant anisotropic strain broadening along the interlayer direction, consistent with the chemistry requiring oxide/hydride substitution in the plane), the S_{202} and S_{022} parameters were weakly negative or positive, and the S_{220} parameter was strongly negative. In the case of the (11l) reflections, the calculated full-width half-maximum (fwhm) is determined by contributions from the S_{400}, S_{040}, and S_{220} parameters. The negative S_{220} compensates for the contribution of the positive S_{400} and S_{040} to produce a relatively narrow peak for the (110) reflection. Overall, these results expose the fact that the (11l) and (00l) classes of reflections are much sharper than the (h0l) and (0kl) reflections.

The use of the Stephens model to fit **2** and **1** presumes that the main contribution to anisotropic peak broadening stems from

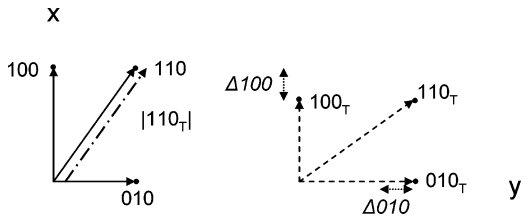

Figure 10. Real-space lattices for ordered and disordered CoOH layers: (a) 100, 110, and 010 d spacings in the ordered material with Co−H bonds along *b* and Co−O bonds along *x* (solid arrows represent the d spacings, and filled circles, the lattice points). The dot−dash line represents the magnitude of d_{110} from case (b) (slightly displaced from the origin to demonstrate that it is identical to the magnitude in case (a)) where interchange of O and H produces a large change in the local repeats along the *x* and *y* directions but none in that along the 110 direction. There is thus a large distribution in d spacings (microstrain) produced by the O/H disorder along *h*00 and 0*k*0 but is considerably reduced along *hh*0, explaining the anisotropic microstrain observed.

a distribution of lattice parameters. The marked changes in the in-plane lattice parameters during the transformation from tetragonal oxide **2** to orthorhombic oxide hydride **1** provide a justification for this phenomenological description of microstrain anisotropy. Qualitatively, this anisotropic broadening may be further understood as a distribution of distances in the CoOH plane due to the transition from a tetragonal oxide to an orthorhombic oxide hydride, the distortion being driven by ordering of oxide and hydride in different orthogonal directions in the *xy* plane. This is a significant observation as it correlates with the evolution of the orthorhombic strain during reaction to demonstrate that the oxide/hydride order along the two orthogonal in-plane directions in **1** evolves during the formation of **1**. Incomplete O/H ordering will produce locally a shortened *a* parameter corresponding to a Co−H rather than a Co−O bond correlated with a lengthened *b* parameter corresponding to a Co−O rather than a Co−H bond. The effect of this is to produce a broad distribution of values for *h*00 and *0k*0 d-spacings when the faulting is extensive; as reflections such as 110 are vector sums of 100 and 010, local disorder of O and H has only a second-order effect on d110, thus producing a considerably reduced distribution of 110 d-spacings compared to those for 100 and 010 (Figure 10) because the lengthening of *b* is correlated locally with the shortening of *a* by the O/H disorder. The enhanced homogeneity of O/H ordering within each ordered domain as the formation of **1** proceeds thus naturally results in a decrease in the anisotropic strain broadening. As this strain mechanism is restricted to the *xy* plane, the microstrain parameters controlling the 00*l* reflections are not significant, consistent with the observations.

Annealing **1** produces a large decrease in the strain imposed by misfit due to defects in the *xy* CoOH plane—this can be attributed to improved O/H ordering in this plane. Even the annealed widths reveal significant anisotropy with the reflections with significant *k* content being broadened over equivalent *h*0*l* ones. This is consistent with the incomplete occupancy of hydride sites along *b* and complete occupancy of the oxide sites along *a* implied by the final composition.

The kinetics of the evolution of the phase fraction of **1** at 450 °C are fitted to the Avrami−Erofe'ev form. In phase-boundary controlled reactions, the exponent $n = \nu + \mu$ where ν is the dimensionality of the growth process and μ is the contribution of nucleation and varies between 0 (where nucleation is instantaneous) and 1 (where it is slow). The observed exponent is thus consistent with either one- or two-dimensional growth. This result is supported by the analysis of the anisotropic peak broadening, which shows that broadening is mainly observed in the *xy* CoOH plane.

The formation of the oxide hydride phase **1** is extremely sensitive to the hydrogen pressure in the reaction vessel. As hydrogen is present in **1**, it is not unreasonable that this should be the case, and detailed investigation may reveal dependence of hydrogen content in the oxide hydrides on hydrogen pressure in the synthetic environment. However, even reduction to form the tetragonal phase **2**, for which analogues have been formed by NaH at lower temperature, is extremely sensitive to hydrogen pressure, proceeding much more slowly under vacuum than in a sealed system. The more rapid reduction in a sealed system is facilitated by reduction of the transition metal oxide with H_2 to form water, which would then be removed from the system by reaction with CaH_2 to form CaO and H_2. This would maintain the pressure in the vessel, while facilitating the reaction of CaH_2 to form CaO. From these results it is clear that the gas phase plays a significant role in the reduction of $LaSrCoO_4$ using CaH_2.

Conclusions

Neutron diffraction data have shown that the magnetic ordering temperature of $LaSrCoO_{3.5-x}H_y$ is 380 K. Comparison of this Neel temperature with that of isostructural oxides with the $n = 1$ RP structure indicates that the exchange interactions mediated by the hydride anion are at least as strong as those mediated by oxide. Consideration of the electronic structure of the hydride and oxide ions indicates that the σ-only frontier orbitals of the hydride anion a should produce purely antiferromagnetic 180° superexchange between Co^{2+} centers, whereas the π and σ contributions from oxide may frustrate each other. The three-dimensional ordering temperature in a layered material is given by the interlayer coupling enhanced by the in-plane correlation length, and so the difference in *c* parameter compared to the oxides is also significant in producing the enhanced antiferromagnetic ordering temperature.

FPLAPW calculations indicate that the electronic structure of $LaSrCoO_3H$ is surprisingly similar to that of $LaSrCoO_4$ once the shift in Fermi energy and lowering in energy of the Co 3d orbitals is taken into account. The 1s orbital of the hydride anion plays a similar role in the electronic structure of **1** to that of the $2p_y$ orbital of the O4 anion in $LaSrCoO_4$ that it replaces in the reaction to form the oxide hydride. A significant amount of mixing occurs between the H 1s orbital, the in-plane O2 $2p_y$ orbital and the Co 3d e_g orbitals. The comparison with $LaSrCoO_4$ and both covalent and ionic hydrides shows that the hydride 1s states do not remain ionic in character at low energy but spread in energy due to covalent mixing to form a complex set of in-plane bonding states involving both the Co 3d x^2-y^2, H 1s, and O 2pσ orbitals. Direct comparison with the bandwidths in DFT calculations with both ionic and covalent hydrides shows the covalency of the H 1s orbitals in the oxide hydride dealt with here. This relates directly to the strength of the superexchange interactions within the CoOH plane and their role in enhancing the Neel temperature of this material in comparison with isostructural oxides.

In situ XRD reveals that a tetragonal phase **2** structurally related to the reduced oxides $LaSrCoO_{3.38-x}$ is a necessary

intermediate in the formation of **1**. In situ evolution of the structures of both **2** and **1** indicate that either the extent of ordering or the hydride concentration in both phases change as the reaction progresses. Evolution of the microstrain anisotropy is consistent with enhanced oxide/hydride/anion vacancy order as the reaction proceeds. A combination of in situ and ex situ results support a reaction mechanism in which a reduced oxide intermediate is initially formed, followed by a substitution of oxide for hydride anions to form the transition metal oxide hydride.

As the oxide hydride **1** is metastable with respect to reduction to elemental cobalt by CaH_2, the ability of Co to form a wide range of tetragonal reduced oxides related to **2** may play a vital role in permitting cobalt to form the first example of an extended transition metal oxide hydride. The relative energies of the cobalt and hydride valence orbitals determine whether the hydride anion remains stable or is oxidized by the metal—less electropositive elements such as copper may simply be too oxidizing to tolerate the presence of hydride, whereas the ability of nickel to adopt the +I oxidation state may lead to the preferential formation of reduced oxides rather than oxide hydrides in the presence of the hydride anion.

Acknowledgment. We thank the EPSRC for Portfolio Partnership support and access to beamtime; we thank Dr. T. Hansen (ILL) and Dr. M. A. Roberts (SRS) for their expert support on the D2B and D20 and 9.1 instruments.

Supporting Information Available: La^{3+}/Sr^{2+} distribution in *Pmm*2 symmetry; experimental details for in situ diffraction experiments; schematic orbital interactions in $LaSrCoO_3H$ and $LaSrCoO_4$; density-of-states comparison between *Pmm*2 and *Imm*2 structures; band structure of $LaSrCoO_4$; estimation of magnetic critical exponent; temperature dependence of unit cell and atomic displacement parameters for $LaSrCoO_3H_{0.7}$; Example Rietveld refinements of neutron diffraction data from D20 and D2b; Thermal expansion coefficients; time dependence of in situ diffraction patterns; evolution of reagent weight fractions at 400 °C; evolution of Bragg reflection fwhm upon annealing; comparison of diffraction patterns of annealed and unannealed samples; chemical information deduced from neutron diffraction data. This material is available free of charge via the Internet at http://pubs.acs.org.

JA042683E